The beneficiation of lunar regolith for space resource utilisation: A review

J.N. Rasera [a,b,*], J.J. Cilliers [a], J.A. Lamamy [b], K. Hadler [a]

[a] Earth Science and Engineering, Imperial College London, SW7 2AZ, United Kingdom
[b] ispace Europe S.A., Rue de l'Industrie 5, L-1811, Ville de Luxembourg, Luxembourg

A B S T R A C T

Space Resource Utilisation (SRU) technology will enable further exploration and habitation of space by humankind. The production of oxygen on the Moon is one of the first objectives for SRU; this can be achieved through the thermo-chemical reduction of the lunar regolith. Several techniques, such as hydrogen reduction and molten salt electrolysis, have been proposed. All reduction techniques require a consistent feedstock from the regolith to reliably and consistently produce oxygen. The preparation of this feedstock, known as beneficiation, is a critical intermediate stage of the SRU flowsheet, however it has received little consideration relative to the preceding excavation, and the subsequent oxygen production stage. This review describes the physics of the main beneficiation methods suitable for SRU. Further, we collate and review all of the previous studies on the beneficiation of lunar regolith.

1. Introduction

Installing a permanent human presence on the Moon or Mars has become a long-term aspiration for both space agencies and private corporations. This can be achieved through the development of technologies that will enable the utilisation of locally-available resources. This is known as Space Resource Utilisation (SRU), and will facilitate both longer-duration and lower-cost space exploration missions.

Lunar SRU was proposed theoretically by Clarke (1950) in the 1950s. During Apollo in the 1960s, SRU was suggested by Carr (1963) as a means to reduce launch mass and terrestrial dependency. Analyses of the samples returned by the Apollo and Luna missions and of remote sensing data collected by lunar orbiters have shown that the Moon is rich in oxygen, hydrogen, metals and silicon but poor in carbon and nitrogen.

The main commodities of interest on the Moon include: oxygen; metals such as titanium, iron, silicon and aluminium; solar wind implanted volatiles, such as helium-3; and, billions of tons of water ice in the polar regions (Sowers, 2016; Colaprete et al., 2010). In situ oxygen production has received the most attention historically from the SRU community, likely due to the numerous applications of oxygen in space.

The end-to-end SRU process for oxygen production, known as the flowsheet, is described by Hadler et al. (2019). The flowsheet is divided into three primary activities:

1. Excavation, where regolith is collected and conveyed;

2. Beneficiation, where regolith is prepared into a suitable feedstock through particle sizing and mineral enrichment; and,
3. Reduction, where the prepared feedstock is reduced and evolved oxygen is captured.

Over a dozen excavation techniques and more than twenty methods for oxygen production from lunar regolith have been proposed in the literature; thorough reviews of these have been performed by Just et al. (2020) and Taylor and Carrier (1993), respectively. The beneficiation stage, however, has largely been overlooked.

This review has three aims: to present the fundamental physics behind beneficiation in the context of lunar SRU; to review critically the findings presented in the literature; and, to identify knowledge gaps in the field. Following the introduction, there are five sections. Section 2 discusses the need for beneficiation in lunar SRU as well as the considerations specific to the lunar regolith and regolith simulants. Section 3 presents the fundamental physics that underpin dry separations. Section 4 summarises and compares the results of laboratory demonstrations of dry mineral enrichment for lunar applications from the literature. Finally, Section 5 presents the identified knowledge gaps.

2. Beneficiation aims and considerations

2.1. Feedstock preparation

In terrestrial mineral processing, beneficiation is critical to the

Nomenclature

			σ	Conductivity $S \cdot m^{-1}$
Constants			τ_b	Time constant for the initial decay of charge s
μ_0	Magnetic permeability of vacuum $4\pi \times 10^{-7} H \cdot m^{-1}$		τ_c	Time constant for the charge back-flow s
ε_0	Vacuum permittivity $8.85 \times 10^{-12} F \cdot m^{-1}$		θ_C	Curie temperature (0 for paramagnetic materials) K
A_H	Hamaker constant $4.3 \times 10^{-20} J$		ε_p	Relative permittivity of particle $F \cdot m^{-1}$
C	Curie constant, material specific K		φ_p	Energy band gap eV
k_B	Boltzmann's constant $8.617 \times 10^{-5} eV \cdot K^{-1}$		ϱ_p	Equivalent total resistance of particle Ω
S	Normalised surface cleanliness Day: $0.88J$, Night: $0.75J$		$\vec{\omega}$	Angular velocity $rad \cdot s^{-1}$
			$\vec{B}$	Magnetic flux density T
Forces			$\vec{E}$	Electrosatic field strength $V \cdot m^{-1}$
$\vec{F}_C$	Coulomb force N		$\vec{g}$	Acceleration due to gravity $m \cdot s^{-2}$
$\vec{F}_g$	Gravitational force N		$\vec{H}$	Magnetic field intensity $A \cdot m^{-1}$
$\vec{F}_m$	Magnetic force N		$\vec{R}_i$	Position of ith particle m
$\vec{F}_p$	Net force on a particle N		$\vec{R}_p$	Position of target particle m
$\vec{F}_{ad}$	Adhesive force N		$\vec{v}$	Velocity of particle $m \cdot s^{-1}$
$\vec{F}_{de}$	Dielectrophoresis force N		C	Capacitance of particle F
$\vec{F}_{vdW}$	van der Waals force N		d_p	Diameter of particle m
			D_{50}	Average particle diameter
Variables			m_p	Mass of particle kg
χ_f	Magnetic susceptibility of fluid $m^3 \cdot kg^{-1}$		N	Number of particle-particle contacts
χ_p	Magnetic susceptibility of particle $m^3 \cdot kg^{-1}$		Q	Final charge on a particle C
ε	Void fraction		Q_c	Total charge in the region of contact during contact C
η_f	Dynamic viscosity of fluid $kg \cdot m^{-1}s^{-1}$		q_i	Charge on ith particle C
Φ_p	Surface potential V		q_p	Charge on target particle C
ϕ_p	Work function of particle eV		r_p	Diameter of particle m
ϕ_s	Work function of surface eV		R_{sep}	Separator radius m
ρ_f	Density of fluid $kg \cdot m^{-3}$		T	Temperature K
ρ_p	Density of particle $kg \cdot m^{-3}$		t	Time s
ρ_{eff}	Effective density $kg \cdot m^{-3}$		t_b	Time between contacts s
ρ_{medium}	Density of particle medium comprising a fluidised bed $kg \cdot m^{-3}$		t_c	Contact time s
			V_p	Volume of particle m^3

economical and profitable operation of all mines. The objective of beneficiation is to produce an optimal feedstock for subsequent metal-

lurgical processing. The majority of metals mined are bound in mineral ores, and account for a small percentage of the material excavated. The
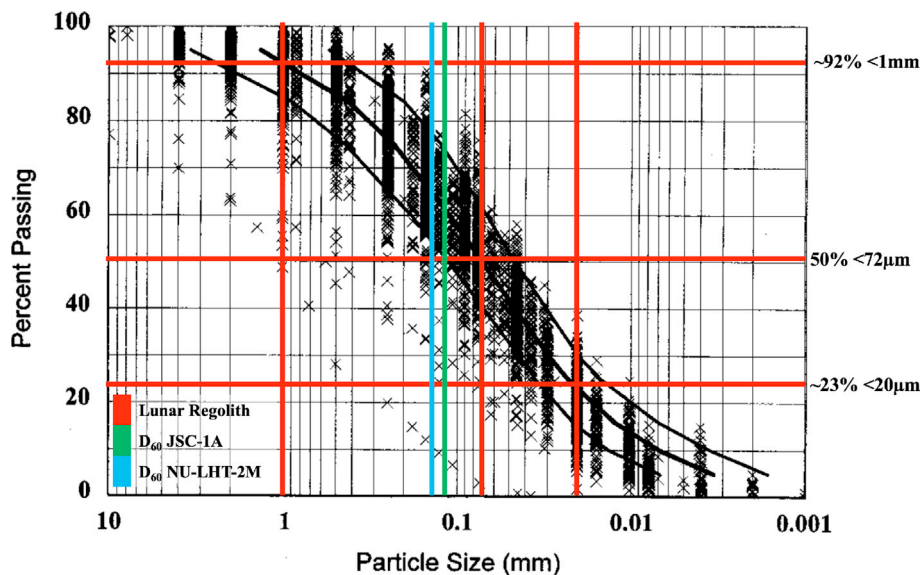

Fig. 1. Particle size distribution of the lunar regolith based on 4500 data points from 350 samples, with the major particle size fractions highlighted. The middle curve shows average distribution, and the left- and right-hand curves show ± 1 standard deviation (Carrier, 2003).

Table 1
Collated properties of Apollo sample 71061,1 converted to *wt*% (Heiken, 1975; Cilliers et al. 2020 Hadler).

Size *μm*	<45	45–90	90–1000	>1000
Total Mass Fraction	30.2	11.4	26.2	32.2
Agglutinates	12.0	9.9	6.9	–
Glass	–	23.8	13.3	–
Basalts	–	13.0	41.5	100.0
Breccia	–	3.5	6.9	–
Other minerals	–	39.6	26.4	–
Ilmenite	–	8.6	4.7	–
Other	88.0	1.6	0.3	–

run-of-mine grade is too low to economically produce metal, thus must be prepared into a consistent, high-grade feedstock prior to smelting. For example, the average global copper grade is 0.62 *wt*.% (Mudd and Weng, 2012), however the smelter requires the grade to be around 30 *wt*.% before it will be accepted (Davenport et al., 2002). To accomplish this, the ore must be enriched by a factor of 48 to make it saleable.

The Moon's surface is covered in a layer of fine soil called regolith. The mineral composition of the regolith varies across the surface, but the two general regions are called Mare and Highlands. The Mare regions, the darker areas on the Earth-facing surface of the Moon, are richer in iron and titanium (French et al., 1991). The Highlands cover the remainder of the near side and the entire far side of the Moon, and are comprised of lighter silicate minerals (French et al., 1991). The minerals that make up the lunar surface all contain oxygen, however the reduction conditions and oxygen yield for each mineral varies.

The four most promising techniques for lunar oxygen production are hydrogen reduction, carbothermal reduction, molten regolith electrolysis and molten salt electrolysis (Schwandt et al., 2012). All of these techniques are in early stages of development, although working reactors for all four have been demonstrated. Hydrogen reduction preferentially reduces ilmenite ($FeTiO_3$), found predominantly in the Mare, whereas the remaining processes are capable of reducing a broader range of minerals,

including silicates. All of these processes require heating the regolith to high temperatures, and consume significant energy.

The regolith is very fine, with an average diameter (D_{50}) of approximately 72 *μm* (Carrier, 2005; French et al., 1991). Particle size distributions for the samples collected by the Apollo and Luna missions is given in Fig. 1 (Carrier, 2005). Over 90% of the regolith comprises particles finer than 1 *mm*, and approximately 23% is finer than 20 *μm*. Further, the modal mineralogy and bulk chemical composition of the regolith is not uniform across all size fractions, as can be seen in Table 1. Depending on the excavation site, mineral enrichment may be possible, to an extent, through sizing alone.

Most reduction processes are not sufficiently advanced to have been optimised to establish the ideal feedstock particle size distribution and composition. Of the designs that have considered feedstock composition, that of Gibson & Knudson (Gibson and Knudsen, 1996) requires the grade of the ilmenite in the feed to be between 80 and 90 *wt*.% and be sized between 20 and 200 *μm*. For example., Apollo sample 71061,1 (Table 1), has an overall ilmenite concentration of 2.2 *wt*.% (French et al., 1991). Considering the mineralogy by size, the net useable ilmenite comprises less than 2 *wt*.%. To make this regolith suitable for reduction, the ilmenite would need to be enriched by a factor of 40 (French et al., 1991; Meyer, 2003).

2.2. Regolith and regolith simulants

The lunar regolith samples available for experimentation are limited, and demand exceeds supply. To address this, lunar soil simulants, mined and produced terrestrially, have been developed for laboratory testing; Taylor et al. (2016) cite 29 offerings. Simulants are made to emulate certain regolith properties, such as mineralogy or cohesiveness, however there is no universal simulant that replicates ideally the regolith and meets all research needs (Taylor et al., 2016). Because simulants come from Earth where mineral formation occurred in the presence of water, they are fundamentally different from lunar samples. Sibille et al. (2006) report that while none of the simulants available replicate the lunar

Table 2
Modal mineralogy, chemical composition and physical property comparison of the recommended simulants compared to Apollo samples. Modal mineralogies are sample-specific, whereas chemical compositions are based on averaged values. Data sources in column headings apply to all underlying, unless otherwise specified.

	JSC-1A	Apollo 14	MLS-1	Apollo 11	NU-LHT-2M	Apollo 16
Modal Mineralogy	Hill et al. (2006)	(Labotka et al., 1980)[a]	Hill et al. (2006)	(Taylor et al., 1996)[b]	Schrader et al. (2009)	(Papike et al., 1982)[c]
Glass	49.3	59.1	–	43.0	30.7	49.7
Feldspar	38.8	17.2	47.5	15.8	54.9	38.7
Pyroxene	trace	10.2	29.6	32.6	6.4	1.0
Olivine	9.0	3.5	3.0	6.5	9.5	–
Ilmenite	trace	0.5	8.0	6.0	0.2	–
Other	2.8	9.1	12.0	0.6	0.6	10.7
Bulk Chemistry	Ray et al. (2010)	Freitas and Gilbreath (1982)	(Hill et al. 2007 Taylor)	Freitas and Gilbreath (1982)	U. S. G. Survey (2008)	Freitas and Gilbreath (1982)
SiO_2	45.7	48.1	42.8	42.5	46.7	45.1
TiO_2	1.9	1.7	6.8	7.7	0.4	0.6
Al_2O_3	16.2	17.4	12.1	13.8	24.4	27.2
FeO	–	10.4	16.3	15.8	–	5.2
Fe_2O_3	12.4	–	–	–	4.2	–
MnO	0.2	0.1	0.2	0.2	0.1	0.1
MgO	9.7	9.5	6.2	8.2	7.9	5.8
CaO	10.0	10.8	11.1	12.1	13.6	15.8
Na_2O	3.2	0.7	2.2	0.4	1.3	0.5
K_2O	0.8	0.6	0.20	0.2	0.1	0.1
PsO_5	0.7	0.5	trace	0.1	0.2	0.1
Cr_2O_3	–	0.2	–	0.3	–	0.1
Physical Properties						
D_{50}; *μm*	100 (Arslan et al., 2009)	65 (McKay et al., 1972)	95 (Perkins and Madson, 1996)	51 (Basu et al., 2001)	90 (Zeng et al., 2010)	105 (French et al., 1991)
Specific Gravity; g/cm^3	2.9 (Alshibli and Hasan, 2009)	2.9 (Carrier et al., 1973)	3.2 (Perkins and Madson, 1996)	3.1 (French et al., 1991)	3.0 (Zeng et al., 2010)	2.5 (Lin et al., 1992)

[a] 90–20 *μm* fraction of sample 14163.
[b] <1000 *μm* fraction of sample 10084.
[c] 1000–90 *μm* fraction of sample 64501.

regolith perfectly, some are better suited for certain types of research than others. Many regolith properties are relevant for SRU, such as particle size, shape and composition.

The modal mineralogy, bulk chemistry, and geotechnical properties of three simulants more commonly employed by the studies presented in this review are presented and compared to their 'equivalent' Apollo samples in Table 2.

3. The physics of dry separations

In this section, the parameters and forces affecting dry separation techniques are presented and discussed in the context of lunar SRU. The material, environmental and processing parameters influencing the forces are also presented.

3.1. Lunar beneficiation

All beneficiation technologies separate minerals from waste using differences in physical properties (e.g., density, surface properties, electromagnetic characteristics). On Earth, gravity-driven beneficiation techniques exploit differences in the mass, density, and/or volume of minerals relative to other ore constituents or process fluids (typically water) to elicit separations. Froth flotation, for example, is commonplace in terrestrial copper mining.

For lunar applications, large-scale, water-intensive methods are not viable: liquid water is not readily available, other process fluids are costly to transport to the Moon, and all fluids will eventually require replenishment. Williams et al. (1979) mention the use of air cyclones and pneumatic tables for particle sizing and enrichment on the Moon. They conclude, however, that these processes would present "a formidable technical problem" to implement, and consider instead electrostatic and magnetic techniques (Williams et al., 1979).

Water consumption aside, the lunar environment is a fundamentally different to that of Earth, as summarised in Table 3 (Gibson and Knudsen, 1985).

To address some of these environmentally-imposed limitations, dry techniques that do not use any process fluid must be considered as a first step on the Moon. Whilst it may be possible in the future to use locally-derived fluids for mineral processing, beneficiation equipment for technology demonstration purposes in the short- and medium-term will require novel solutions.

3.2. Force balance

The net force acting on a particle undergoing dry separation is given by the sum of the forces acting on the particle, $\overrightarrow{F}_p$, or:

$$\overrightarrow{F}_{net} = \sum \overrightarrow{F}_p = \overrightarrow{F}_g + \overrightarrow{F}_{ad} + \overrightarrow{F}_{vdW} + \overrightarrow{F}_{char} \tag{1}$$

The first three terms, $\overrightarrow{F}_g$, $\overrightarrow{F}_{ad}$ and $\overrightarrow{F}_{vdW}$ are process-agnostic and impact all beneficiation technologies; the remaining term, $\overrightarrow{F}_{char}$, refers to the characteristic force(s) specific to each separation method. The magnitude of this force will vary depending on the mineralogical, chemical and electromagnetic properties of each particle.

3.3. Universal factors

The gravitational force, $\overrightarrow{F}_g$, experienced by a given object on the Moon is one-sixth of what it would experience on Earth. The majority of the lunar beneficiation techniques presented in the literature depend on the pull of gravity to draw particles through the equipment (Adachi et al., 2017a; Kawamoto and Seki, 2004; Agosto, 1981, 1983, 1984, 1985; Trigwell et al., 2009, 2012; Captain et al., 2007; Quinn et al., 2012).

The adhesive force, $\overrightarrow{F}_{ad}$, is an inter-particle electrostatic force that varies depending on whether a charged particle is in the proximity of another charged or neutral particle. As the lunar regolith is highly-charged and very fine, the adhesive force can become dominant (Adachi et al., 2016). In interactions between two charged particles, the adhesive force is found by (Afshar-Mohajer et al., 2011a; Manouchehri et al., 2000a):

$$\overrightarrow{F}_{ad} = \frac{q_p}{4\pi\varepsilon_0} \sum_{i=1}^{n} \frac{q_i(\overrightarrow{R}_p - \overrightarrow{R}_i)}{\left|\overrightarrow{R}_p - \overrightarrow{R}_i\right|^3} \tag{2}$$

When charged particle and a neutral one interact, the adhesive force occurs due to charge polarisation within a neutral particle, resulting in a lower magnitude (Bailey, 1984). This is described by:

$$\overrightarrow{F}_{ad} = \frac{q_p^2\left(1 - \frac{\overrightarrow{R}_p - \overrightarrow{R}_i}{\left(r_p^2 + (\overrightarrow{R}_p - \overrightarrow{R}_i)^2\right)^{1/2}}\right)}{16\pi\varepsilon_0\left(\overrightarrow{R}_p - \overrightarrow{R}_i\right)} \tag{3}$$

When considering a pair of neutral particles, the adhesive force would be zero.

The last term, $\overrightarrow{F}_{vdW}$, describes the van der Waals force between particles. Following Scheeres et al. (2010), this interaction can be modelled by:

$$\overrightarrow{F}_{vdW} = \frac{A_H S^2 (r_{p1} r_{p2})}{48\Omega^2 (r_{p1} + r_{p2})} \tag{4}$$

where Ω is the diameter of an oxygen atom ($\Omega = 1.32 \times 10^{-10}$ m), considered to be the minimum separation of two particles on the Moon

Table 3
An adapted comparison of the effects of the lunar environment on processing by Gibson & Knudson (Gibson and Knudsen, 1985).

Feature	Comparison	Impact
Gravity	Moon: 1/6g Earth: 1g	Impacts density separations; Reduces gravity-driven fluid/particle flow; Reduces particle inertia, thus reducing the magnitude; of any external force required to overcome it.
Surface Temp. Day/Night	Moon: 127 °C(D); −173 °C(N) Earth: 14 °C (D/N)	Temperature variation will affect particle properties; Hot particles more easily charged, but less magnetically susceptible and vice versa; Equipment must survive the lunar night.
Atmosphere	Moon: Hard Vacuum Earth: Abundant	Process fluids not readily available, and must be generated *in situ*, or imported from Earth; Fluids, if any, must be used in a closed system; Cooling of equipment (e.g., electromagnets) only possible via heat pipe or radiative exchange.
Human Access	Moon: None Earth: Abundant	High-reliability (uncommon in terrestrial mining) is necessary; Modular designs will facilitate repairs/replacements
Day/Night Cycle	Moon: approx. 324 h Earth: approx. 12 h	Regolith becomes less charged at night (no UV charging); Equipment cooling/heating is power-intensive. Power generation at night becomes challenging

([Perko et al., 2001](#)).

Perko et al. (2001) note that the Moon has a high surface cleanliness (S, the ratio of the diameter of an O_2 ion to the thickness of a layer of adsorbed gases on the particle surface; $S \rightarrow 1$ for a clean surface, and $S \rightarrow 0$ for an unclean one). As a result, the inter-particle spacing on the Moon is very small, implying that the van der Waals force is dominant. This is supported by the experimental work of Izvekova & Popel ([Izvekova and Popel, 2013](#)) for lunar particles below 50 μm; larger particles, however, were found to experience a dominant adhesive force.

3.4. Electrostatic terms

Electrostatic separation considers two characteristic forces: the Coulomb force and the dielectrophoresis force. The Coulomb force acts on charged particles in any electrostatic field, whereas the dielectrophoresis force acts on neutral particles in non-uniform fields.

Coulomb force separation techniques require charged particles to be passed through an electrostatic field ([Knoll and Taylor, 1985](#)); positively-charged particles will be repelled by the positive electrode, and vice versa. The magnitude of the Coulomb force on a particle, $\overrightarrow{F}_C$, is given by ([Kelly and Spottiswood, 1989a, 1989b, 1989c](#); [Manouchehri et al., 2000a](#)):

$$\overrightarrow{F}_C = q_p \overrightarrow{E} \tag{5}$$

The dielectrophoresis force acts through the polarisation of neutral particles in non-uniform electrostatic fields. As a result, it is typically small relative to the Coulomb force, and is insignificant over large distances ([Bailey, 1984](#)). Following [Pohl, 1951, 1958, 1960, 1978](#), [Jones (1979)](#), [Washizu (1993)](#), and Washizu & Jones ([Washizu and Jones, 1994](#)), this force is given by:

$$\overrightarrow{F}_{de} = 2\pi r_p^3 \varepsilon_0 \left(\frac{\varepsilon_p - \varepsilon_0}{\varepsilon_p + 2\varepsilon_0} \right) \nabla \overrightarrow{E}^2 \tag{6}$$

[Ballantyne (2011)](#) and Ballantyne et al. ([Ballantyne and Holtham, 2010, 2014](#)) have demonstrated that dielectrophoresis can be used for mineral separations for terrestrial applications, however it has not been demonstrated for lunar applications on its own.

Particle shape has been shown to play a role in electrostatic separation, particularly in the food, recycling and toner industries ([Miller and Barringer, 2002](#); [Lu et al., 2008](#); [Galliford, 2005](#)). It has been discussed in the context of tribocharging in terrestrial mineral processing by Ireland ([Ireland, 2010a, 2010b, 2012](#); [Ireland and Nicholson, 2011](#)) and Knoll & Taylor ([Knoll and Taylor, 1985](#)). Ireland's ([Ireland, 2012](#)) tribocharging model suggests that irregular particles tumbling down an incline attain a higher change than those that slide on one plane. For lunar applications, Izvekova & Popel ([Izvekova and Popel, 2013](#)) found that the presence of asperities attenuated the adhesive force by two to three orders of magnitude ([Izvekova and Popel, 2013](#)). The impact of the differences in particle shape between real regolith and regolith simulants on particle charging has not been presented in the literature.

Whilst the lunar regolith possesses a natural electrostatic charge at the surface, the magnitude has not yet been characterised *in situ* nor has been the depth at which charged particles exist. It may be possible to take advantage of this natural charge to demonstrate electrostatic separation on the Moon, however the regolith simulants used for lab testing do not possess a natural static charge. To address this, induction charging, tribocharging, ion and electron bombardment, and UV exposure have been proposed in the literature as means of imparting charge, and are discussed herein.

3.4.1. Induction charging

Induction charging occurs when uncharged particles pass through a non-ionising electrostatic field and acquire the polarity of that field ([Kelly and Spottiswood, 1989b](#)). If a conducting or semi-conducting polarised particle then contacts an earthed surface, it loses one polarity

to the conductive surface resulting in a net charge of opposite polarity ([Kelly and Spottiswood, 1989b](#)). Non-conductive particles assume no net charge, thus are neither attracted or repelled by the field.

The charge on an individual particle can be approximated empirically by ([Afshar-Mohajer et al., 2011b](#); [Stubbs et al., 2006](#); [Horányi, 1996](#)):

$$q_p = C\Delta\Phi_p \tag{7}$$

This can be expanded to model the charge acquired by induction as particles pass through a non-ionising electrostatic field ([Kelly and Spottiswood, 1989b](#); [Barthelemy, 1960](#)):

$$q_p = C\Delta\phi_p \left[1 - e^{-t/\rho_p C} \right] \tag{8}$$

Capacitance has been approximated by [Goertz (1989)](#) and [Afshar-Mohajer et al. (2011b)](#) by:

$$C = 2\pi\varepsilon_0 d_p \tag{9}$$

[Manouchehri et al. (2000b)](#) specify that the conductivity of a mineral at a given temperature, σ, is related to the temperature, T, by:

$$\sigma = \sigma_0 exp^{-\frac{\varphi_p}{2k_B T}} \tag{10}$$

where σ_0 is a constant dependent on the density and mobility of electrons and holes in the material ([Gao et al., 2011](#)).

As the temperature of a mixture of non-conductive particles is increased, some species may become sufficiently conductive to allow for separation by conductive induction ([Manouchehri et al., 2000b](#)). Materials with very high resistivity and low conductivity (e.g. minerals) are difficult to separate in conductive induction devices since they will not acquire sufficient charge quickly enough to produce a separation ([Fraas, 1962](#)). Raising the temperature increases the conductivity of the particles, and makes it possible to induce a stronger charge ([Fraas, 1962](#); [Lindley and Rowson, 1997a](#)).

3.4.2. Tribocharging

Tribocharging is a process by which particles (conductors, semi-conductors and insulators) acquire charge through frictional rubbing and subsequent separation. The magnitude of the final charge on each particle after they have separated is the product of the charge that is transferred during the contact and the charge back-flow experienced once the particle-particle contact is broken ([Kelly and Spottiswood, 1989b](#)).

The transfer of charge is defined using the Fermi level ([Manouchehri et al., 2000a](#)): when a particle with a higher Fermi level (lower work function) contacts a material with a lower Fermi level (higher work function), the former will lose an electron and the latter will gain it. The contact charging of metals is directly related to the difference in Fermi level ([Schein, 2007](#)); the contact charging of insulators, however, is not well understood.

Insulator-insulator charging has been the focus of a number of studies in fields ranging from electrophotography to pharmaceutical powder processing ([Kelly and Spottiswood, 1989b](#); [Schein, 2000, 2007](#); [Gooding and Kaufman, 2011](#); [Zafar et al., 2018](#); [Liu and Bard, 2008, 2009a, 2009b, 2010](#)). To explain the phenomenon, three mechanisms have been proposed: electron transfer, ion transfer and material transfer ([Gooding and Kaufman, 2011](#)). There is no consensus on which mechanism is dominant, and may be system-dependent. Gooding & Kaufmann ([Gooding and Kaufman, 2011](#)) present a thorough analysis and discussion of the problem, and conclude that molecular-scale investigations will be necessary in order to understand it. As a result, [Baytekin et al. (2011)](#) and [Lacks (2012)](#) suggest that a universal tribocharging model may not exist.

Whilst the Fermi level of materials largely governs the transfer of charge, particle size, shape and angularity, lattice defects, surface contamination, ion and water adsorption, dielectric constant, type of contact, and number and duration of contacts all impact the amount of charge transferred ([Manouchehri et al., 2000a](#)). As noted by Kelly and

Spottiswood (Kelly and Spottiswood, 1989b) and Manouchehri et al. (2000a), the number of factors involved make the electrification process complex. Further, few electromagnetic properties of regolith minerals, such as permittivity, have been reported in the literature for terrestrial samples, let alone lunar ones. Of those that are characterised, the data are often not in agreement. For example, Ballantyne and Holtham (2010) summarise eight permittivity measurement studies for a number of terrestrial minerals: while the majority of the examples presented are generally within the same order of magnitude, no two studies present identical measurements.

Despite the lack of clarity on the underlying mechanism of charge transfer, the maximum available charge following a particle - particle or particle - tribocharger interaction can be modelled with satisfactory agreement to empirical data. The Harper equation employs differences in work functions to determine charge transferred per unit mass (Manouchehri et al., 2000a):

$$\frac{q_{p,max}}{m} = 2.66 \times 10^{-13} \left(\frac{\phi_s - \phi_p}{\rho_p r_p^2} \right) (8.85 + 1.151 \log_{10} r_p) \tag{11}$$

where $q_{p,max}/m$ is the maximum charge to mass ratio in $C \cdot kg^{-1}$.

The amount of charge transferred can also be modelled as a function of the number and duration of particle contacts; both of these variables, however, can only be approximated for any given system. This is given by (Kelly and Spottiswood, 1989b; Lindley and Rowson, 1997b):

$$\frac{dQ_N}{dN} = Q_c \left(1 - e^{-t_b/\tau_b} \right) - Q_N \left(1 - e^{-t_c/\tau_c} \right) \tag{12}$$

$$Q(N) = k_1 - k_2 e^{-Nk_3} \tag{13}$$

where k_1, k_2 and k_3 are empirically-derived constants.

Tribocharging is the simplest method considered for imparting charge on particles, making it an attractive option for lunar SRU, however it is challenging to characterise experimentally on Earth due to extreme environmental differences. Early *in situ* demonstrations on the lunar surface will be necessary.

3.4.3. Ion, electron and UV bombardment

Ion bombardment employs a corona-generating electrode mounted above an earthed metallic surface and a gas to ionise (Knoll and Taylor, 1985; Kelly and Spottiswood, 1989a, 1989b, 1989c; Mora, 1958). As particles pass under the corona, the ionised gas impinges upon them and transfers charge. When the particles exit the corona, conductive materials lose any charge to the earthed surface, rendering them neutral, whereas semi- and non-conductors will be polarised. The polarised particles 'see' an image charge in the earthed surface, and adhere to the that plane (Fig. 2). In roller separators (Fig. 3), the neutral conductors are then flung from the surface of the roller, and end up in the farthest collection hoppers, whereas the semi- and non-conductors end up in closer hoppers, or remain adhered to the surface (see Fig. 3).

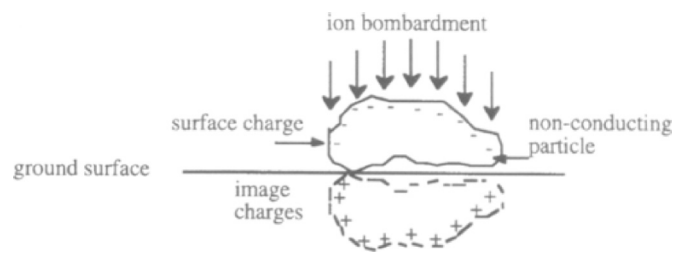Ion bombardment is commonly used in terrestrial beach sands

Fig. 2. A conducting particle will lose its charge to the neutral roller and be ejected instead of being attracted to an image charge (Kelly and Spottiswood, 1989a).
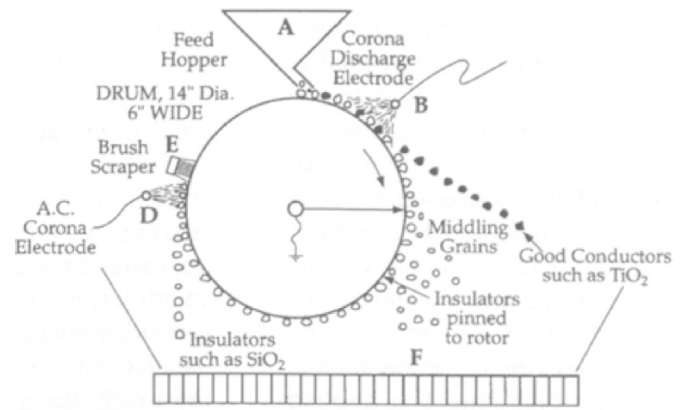

Fig. 3. Earthed drum separator (Manouchehri et al., 2000a).

processing for the separation of ilmenite and rutile from quartz, the food processing industry, and the recycling industry (Knoll and Taylor, 1985; Brands et al., 2001; Lawver et al., 1986). While it has not been studied directly for use in SRU, Agosto (1985) noted that gas ionisation likely contributed to the superior performance of his apparatus under air and nitrogen than vacuum. The production and ejection of ions in space is not uncommon; ion thrusters are used regularly for satellite station keeping. Similar technology could be employed for particle charging in lunar SRU.

Electron beam charging has a lower energy requirement to produce the beam compared to that required for gas ionisation (Kim and Elsayed-Ali, 1982). Additionally, it eliminates the need for an ion source. The charging of granular material under vacuum using ion, electron and UV bombardment was demonstrated by Wang et al. (2016) to explain particle transport on airless bodies. In their experiments, silica-rich Martian regolith simulant composed of 38–48 μm particles was charged using a combination of ions and electrons, electrons only, and UV exposure (Wang et al., 2016). They found that the charge imparted on the samples by the electron beam was an order of magnitude greater than the combined ion/electron bombardment, and three orders of magnitude greater than the UV method ($q_{elec} = 2.3 \times 10^{-16} C$ vs. $q_{combi} = 2.8 \times 10^{-17} C$ vs. $q_{UV} = 5.5 \times 10^{-19} C$).

For charging regimes that impinge ionised particles, electrons or UV on a feed, the Pauthenier Limit (Pauthenier and Moreau-Hanot, 1932; Goldwater et al. 2019 Millen) can be employed to determine the theoretical maximum charge on a spherical particle, as follows:

$$q_{p,max} = 4\pi r_p^2 \varepsilon_0 p |\vec{E}| \tag{14}$$

where p is a constant ($p = 3$ for conductors and $p = 3\varepsilon_p/(\varepsilon_p + 2)$ for dielectrics).

3.5. Magnetic terms

Materials can be categorised by the way in which they interact with magnetic fields; they are classed as diamagnetic, paramagnetic or ferromagnetic.

Many of the minerals on Earth and the Moon are diamagnetic. These minerals interact only with very strong magnetic fields, and when such a field is present, they oppose the field instead of being attracted by it (Parodi, 1996; Rosenblum and Brownfield, 2000; Jackson, 2015). All materials have a diamagnetic component to their magnetic makeup, however it is only the dominant component amongst minerals and materials that do not bear iron (Parodi, 1996).

Minerals that demonstrate paramagnetism, such as ilmenite (Rosenblum and Brownfield, 2000), are made up of atoms with unaligned magnetic moments. These moments react independently to applied magnetic fields and thermal energy (Butler, 2004). Without an applied magnetic field, the moments are randomly oriented, and thus results in

net zero magnetisation (Butler, 2004). In general, strong magnetic fields are required to separate paramagnetic materials from an otherwise non-magnetic feedstock; for many paramagnetic materials, a magnetic field of at least 2 T is necessary (Svoboda, 1994; Wills and Finch, 2015).

Ferromagnetic materials are strongly susceptible to magnetic fields, and can become highly magnetised (Chikazumi and Graham, 2009). Ferromagnetic materials can be separated with low-intensity magnets because of their strong interaction with magnetic fields. Metals that exhibit ferromagnetism include iron, nickel and cobalt, as well as many of their alloys; naturally ferromagnetic minerals include those within the titanomagnetite and titanohematite series (Butler, 2004), however there is not any strong evidence of their existence on the Moon (Fuller, 1974; Strangway and Olhoeft, 1977).

There is only one characteristic force to be considered in magnetic separation: the magnetic force, $\overrightarrow{F}_m$. This can be modelled for para- and ferromagnetic materials by:

$$\overrightarrow{F}_m = V_p \rho_p \left(\chi_p - \chi_f\right) \overrightarrow{H} \frac{d\overrightarrow{B}}{dx} \qquad (15)$$

Magnetic susceptibility, χ_p, follows the Curie-Weiss Law and is inversely proportional to temperature, as follows:

$$\chi_p = \frac{C}{T - \theta_C} \qquad (16)$$

The magnetic susceptibility will decrease with increasing temperatures, adversely affecting magnetic separations (Dahlin and Rule, 1993).

As there are no minerals in the lunar regolith that produce a magnetic field themselves (such as magnetite), inter-particle magnetic attraction is disregarded.

4. Lunar mineral beneficiation studies

Following the physics that governs dry separations, this section reviews the application of separation techniques to lunar minerals.

4.1. Electrostatic separations

Three techniques have been demonstrated in the literature for lunar mineral beneficiation through manipulating electrostatic forces: conductive induction with slide separators, tribocharging with parallel plate separators, and the electrostatic travelling wave.

4.1.1. Conductive induction with slide separators

Agosto, 1983, 1984, 1985, 1992 has produced the largest body of work on the use of conductive induction for lunar SRU.

Following a comparison of slide-type and roller-type separators on binary mixtures of minerals in air (ilmenite/olivine, anorthite/pyroxene, and olivine/anorthite), Agosto found that the slide-type was superior in performance (Agosto, 1983). Using a mixture of ilmenite and olivine in a ratio of 10:90 by mass in four size fractions, the slide separator was found to produce higher grades of ilmenite after one pass compared to the drum type, albeit with lower recovery (see Table 4). If the gangue were to be reprocessed subsequently, the overall recovery would be expected to

increase (Agosto, 1983). All further testing performed by Agosto employed the slide-type separator for its stronger performance and for its ease of use under vacuum conditions (Agosto, 1984).

Agosto found the separation efficiency was improved by elutriation of each sample in isopropyl alcohol or TP-35 (a mixture of Freon and isopropyl alcohol). Cleaning the samples in this fashion allowed for the removal of the <45 μm fraction and drove off any adsorbed water (Agosto, 1983). All subsequent testing ((Agosto, 1984; Agosto, 1985)) employed the same process on all fabricated simulants. It is not clear whether this cleaning process was performed on the Apollo samples used in subsequent tests, or if it was only meant for simulants (Agosto, 1984, 1985).

The binary mixtures were tested both at room temperature and at 180 °C. It was found that the higher temperature greatly improved both the grade and recovery, as shown in Table 5 (Agosto, 1983). The higher temperature was found in all cases to improve the separation of the pre-treated samples; for semi-conductors, the increase in temperature results in an increase in conductivity, and for all minerals, temperatures exceeding 100 °C prevented water adsorption. All tests therefore maintained the feedstock, vibratory feeder and slide between 100 and 200 °C with infrared heaters (Agosto, 1983, 1984, 1985).

The feeds were passed into the separator at a rate of approximately 6 g/s (7 g/s for the binary mixtures), with 1–5 g of material used in air and a few hundred milligrams in the nitrogen and vacuum arrangements (Agosto, 1983, 1985).

When studying the binary mixtures, two maximum field strengths, +7 and + 4.7 kV/cm were used; recovery was found to be most strongly affected by this, improving by over 100% in some cases (Agosto, 1983), and is in agreement with testing performed by Inculet et al. (1972). In subsequent testing, the induction charging electrode was maintained nominally at +5 kV, but ranged between 2.5 and 7 kV (Agosto, 1984, 1985). While the semi-conductors were charged via induction, they also gained charge through contact with the aluminium slide (tribocharging); stochastic differences in conductivity between particles of the same type could therefore result in either tribocharging or induction charging imparting the dominant charge.

For example, semi-conductive pyroxene was found to gain a negative contact charge through contact with the slide. When a negative polarity was applied to the separating electrode (thus inducing a positive charge in conductive particles), less conductive pyroxene particles would gain a net negative charge from the slide, whereas more conductive ones would attain a net positive charge through induction. The negatively charged pyroxene would either adhere to the slide or end up in the non-conductor hopper, whereas the conductive particles reported to the conductor hopper.

When a positive polarity was used, 81% of the pyroxene reported to the middlings and conductor hoppers with an average grade of 95% (Agosto, 1983). A comparison of the results is found in Fig. 4. In subsequent tests, a positive polarity was chosen for the separating electrode to augment the negative tribocharge gained by ilmenite via contact with aluminium (Agosto, 1984, 1985).

Following his work on binary mixtures, Agosto, 1984, 1985 used a custom simulant composed of anorthite, ilmenite, olivine, and augite pyroxene in a ratio of 4:1:1:4 by mass (also known as simulant KSC-1),

Table 4
Comparison of drum- and slide-type electrostatic separators on a binary mixture of ilmenite and olivine after one run. Starting ilmenite concentration: 10 wt.% (Agosto, 1983).

Size Fraction [μm]	Drum		Slide	
	Grade [wt.%]	Recovery [wt.%]	Grade [wt.%]	Recovery [wt.%]
45–90	29	29	98	29
90–150	53	64	90	38
150–250	78	91	95	68
250–500	80	87	79	82

Table 5
Effect of heating the feed and air on grade and recovery (Agosto, 1983).

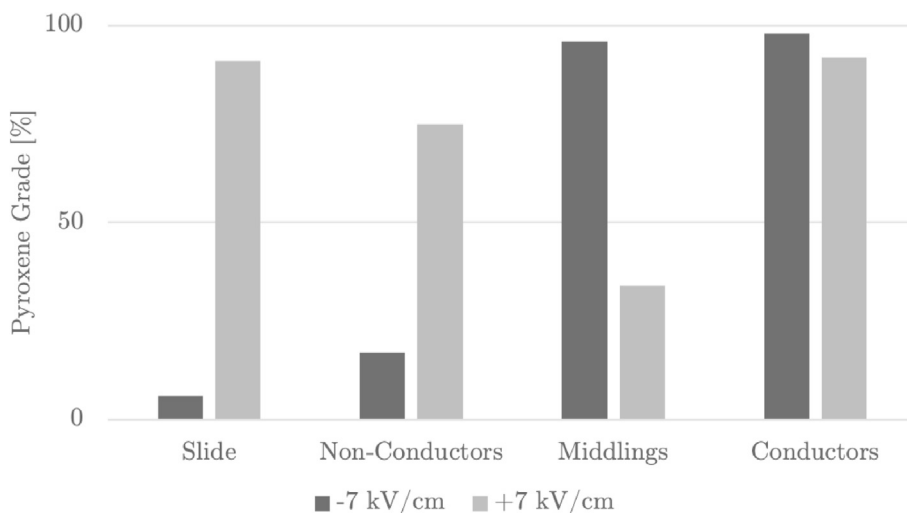| Sample	Size Fraction [μm]	28 °C		180–190 °C	
		Grade [wt-%]	Recovery [wt-%]	Grade [wt-%]	Recovery [wt-%]
Anorthite/ Pyroxene [50/50]	90–150	60	<1	73	54
Olivine/ Anorthite [10/90]	150–250	66	1	94	34

Fig. 4. Grade distribution of pyroxene after separating a 50/50 pyroxene/olivine mixture using positive and negative polarties on the high-voltage electrode. Reproduced from (Agosto, 1983).
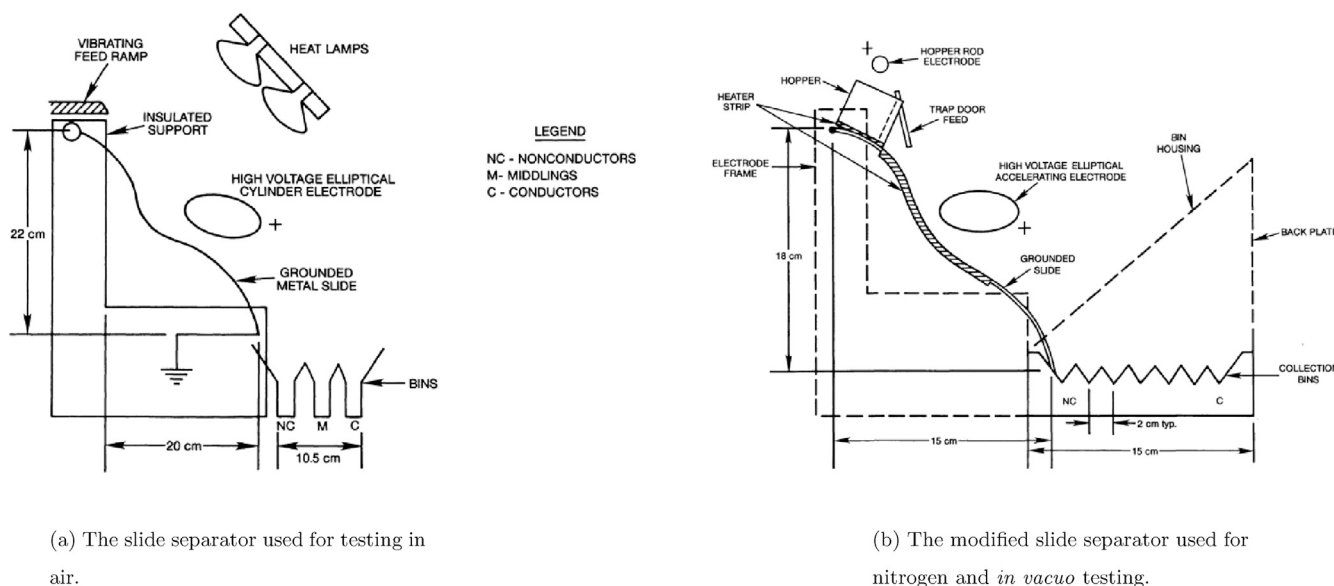

(a) The slide separator used for testing in air.

(b) The modified slide separator used for nitrogen and *in vacuo* testing.

Fig. 5. Agosto's slide separators (Agosto, 1985).

sized to 90–150, 150–250 and 250–500 μm fractions. Additionally, the 90–150 μm fraction Apollo 11 sample 10084,853 was tested for comparison (Agosto, 1984, 1985, 1992). These tests were performed in air at atmospheric pressure, as well as under nitrogen at 1 *torr* and under vacuum at 10^{-5} *torr*. The slide configurations used are shown in Fig. 5a and b.

Ilmenite was enriched under atmospheric conditions from 8.8 wt% to 89 ± 6 wt% with a recovery of 51 ± 9 wt%. This was improved under nitrogen, where the ilmenite was enriched from 7.9 to 90 ± 7 wt% with a recovery of 67 ± 5%. Under vacuum, however, there was an improvement over air, but not as strong as under nitrogen: 9.8 wt% was enriched to 78 ± 8 wt% with a recovery of 56%. The Apollo sample was enriched from 7.3 to 51 wt% with a recovery of 35% under nitrogen and 7 to 29 wt% with a recovery of 55% under vacuum (Agosto, 1985).

Agosto has attributed the higher success rate of the experiments conducted in air and nitrogen to 5 factors: 1) ionised gas may have contributed to particle charging; 2) the lack of vibratory feeder in the vacuum tests may have reduced contact and induction charging

efficiency; 3) fluid drag may have contributed to partial density segregation of ilmenite; 4) fluid drag would have increased the transit time of material in the electrostatic field resulting in greater charge; and 5) the experimental apparatus used was not designed to accommodate the changes in particle motion in the absence of fluid drag (Agosto, 1985).

Whilst Agosto's work has demonstrated the feasibility of conductive induction and slide separators for lunar mineral beneficiation, two outstanding points were not addressed, nor have they been considered through subsequent study. The electrostatic enrichment of mineral fines (i.e., <45 μm) has not been explored for space applications, although both Agosto (1983) and Inculet et al. (Inculet, 1979) suggest that operating under vacuum conditions should make it feasible. Considering that this fraction accounts for approximately 40% of the regolith, fines enrichment is an important area for further study. The natural charge possessed by the regolith has also not been considered, and may ultimately require design adaptations to be made to account for it; however, since this has never been quantified, subsequent designs should consider a wide range of feedstock charges.
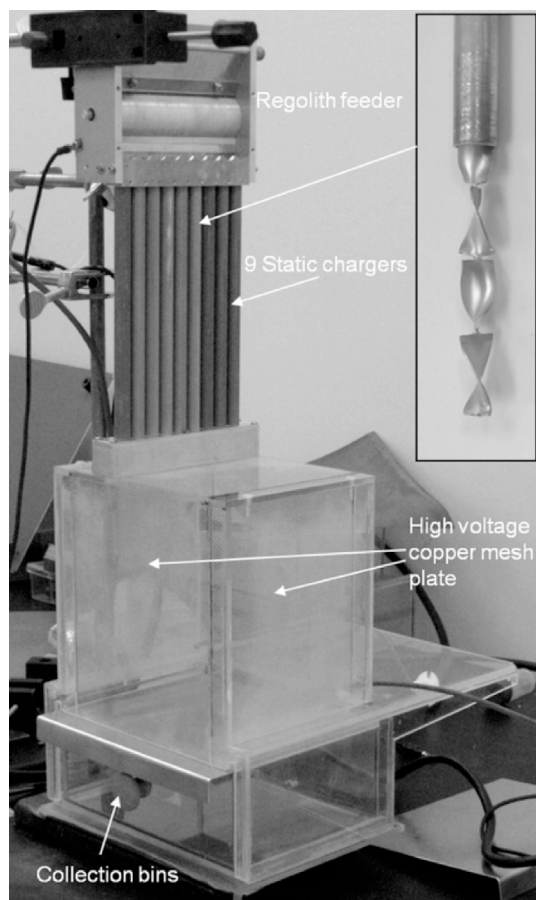
Fig. 6. The free fall triboelectric separator employed by Quinn et al. Regolith simulant is fed into the separator through a series of baffled channels. Different baffle materials are used to impart differing magnitudes of charge on the particles (Quinn et al., 2012).

4.1.2. Tribocharging and plate separation

Plate separators employ pairs of electrodes oriented parallel to one another (for the generation of uniform electrostatic fields) or on an angle relative to the central plane (for non-uniform fields). The plates are typically oriented vertically so that gravity draws particles through the field; pneumatically- or mechanically-assisted systems, however, have been developed with horizontal electrodes (see (Gupta et al., 1993; Bittner et al., 2014)). The use of plate separators for lunar applications has been explored by Li et al. (1999), as well as by Trigwell and colleagues at NASA's Kennedy Space Center (Trigwell et al. (2009; 2012; 2006), Quinn et al. (2012), Captain et al. (2007)).

Li et al. (1999) employed a pneumatically-driven vertical parallel plate separator with a copper tribocharger. The group performed tests on individual minerals (ilmenite, albite, augite, fosterite and quartz), on binary and ternary mixtures, and on a custom regolith simulant. All tests were on material sized to 75–106 μm (Li et al., 1999). Testing individual minerals allowed the authors to qualitatively predict the triboelectric series for their chosen minerals by measuring charge magnitude and polarity. They found that the series progressed as follows (from highest work function to lowest): quartz > augite > albite > ilmenite > copper > fosterite. This data was then used to predict the interactions between particles in the more complex mixtures with reasonable accuracy. For example, they were able to predict that the presence of fosterite in the simulant caused ilmenite to attain little, if any, charge. When measured, they found that the majority of the ilmenite was captured in the central collection zone (Li et al., 1999). Importantly, the authors note that particle-particle interactions more strongly influence the charging behaviour than particle-wall interactions, however it is unclear to what

Table 6
Surface composition of the unbeneficiated JSC-1 stimulant compared to the measured surface composition of the material collected at each electrode as determined by XPS analysis (Captain et al., 2007).

	Surface Composition [%]				
	Al	Na	Fe	Ca	Ti
Raw JSC-1	6.4	4.4	2.5	1.8	0.6
−15 kV	6.6 (+3%)	3.0 (−31%)	5.4 (+8.6%)	2.9 (+13%)	Not Detected
+15 kV	5.7 (−11%)	4.7 (+5.7%)	2.1 (−18%)	1.9 (+4%)	Not Detected

extent pneumatic mixing influences this.

Trigwell et al. (2006) initially employed a pneumatically-driven plate separator with vertical electrodes angled away from the central plane by 4° charged to ±15 kV. Horizontal static mixers (tribochargers) made of aluminium and PTFE were used to charge MLS-1 samples in two size fractions (<25 μm and >100 μm). Material was collected on both the surface of the electrode and in a collector directly below it. The larger fraction was found to charge more successfully than the smaller fraction. The <25 μm sample was split 52%–48% positive to negative with the PTFE charger, whereas the larger fraction was split 14%–86% (Trigwell et al., 2006). This was likely due to the larger particles not adhering to the charger (Trigwell et al., 2006).

Experiments performed on the 50–75 μm fraction of JSC-1 are reported by Captain et al. (2007) (of Trigwell's group at NASA). In this iteration, the pneumatic conveyor was replaced with a free-fall set-up. The samples were tribocharged by falling through an aluminium block with a zig-zag path machined into it. The tests were conducted under vacuum as well as in air. Otherwise, the electrodes and collectors remained the same.

The initial sample and the material collected at each electrode was analysed with XPS and Raman spectroscopy; modal mineralogy was not assessed. The minerals detected in the control and separated fractions were ilmenite ($FeTiO_3$), anatase (TiO_2), magnetite (Fe_3O_4), hematite ($\alpha - Fe_2O_3$), ferrite ($M2^+Fe_2O_3$), olivine ((Mg, Fe)$_2SiO_4$), plagioclase ($NaAlSi_3O_8/CaAl_2Si_2O_8$), and pseudobrookite ($Fe_2TiO_5$). The initial XPS findings, and the post-beneficiation measurements are presented in Table 6. The results indicate that: 1) minerals with higher amounts of iron (namely magnetite and pseudobrookite) tended to charge positively, although ferrite was predominantly observed to charge negatively; 2) a marked increase at the negative electrode in the concentration of calcium and decrease in sodium indicates that the plagioclase was composed of both plagioclase albite ($NaAlSi_3O_8$), which charges negatively, and anorthite ($CaAl_2Si_2O_8$), which charges positively.

Trigwell et al. (2009) compared the performance of copper, aluminium and PTFE for the tribocharging of the 50–75 μm fraction of JSC-1, JSC-1A and KSC-1. Parallel electrodes charged to ±15 kV were employed, and the tribochargers used were machined in the same manner as those used by Captain et al. (2007). Again, XPS was used to evaluate the surface composition of the materials before and after beneficiation; measurements were taken for five runs and averaged. The results of these experiments, found in Table 7, show that the tribocharging and plate separation apparatus was able to successfully enrich titanium-rich ilmenite from the KSC-1 simulant. The results for the JSC-1 and -1A simulants show some notable variations in particle surface composition following beneficiation, but without either the Raman spectroscopy measurements or some other type of modal mineralogy assessment, it is challenging to draw detailed conclusions with respect to the equipment's capacity for mineral enrichment.

Trigwell et al. (2012) go on to modify their experimental apparatus to improve its flexibility: a series of aluminium, copper and PTFE tubes with internal baffles replace the machined charging blocks; up to 7 collection bins can be used; and, the electrode voltage can be increased to ±30 kV

Table 7
XPS measurements for raw and beneficiation JSC-1, JSC-1A and KSC-1; percentage change from unbeneficiated in brackets (Trigwell et al., 2009).

Simultant	Charger	Fraction	Practice Surface Composition [%]					
			Si	Al	Na	Fe	Ca	Ti
JSC-1	Raw	n/a	13.8	6.4	4.4	2.5	1.8	0.6
	Al	Positive Electrode	13.8 (−)	5.2 (−19%)	4.4 (−)	1.9 (−25%)	1.8 (−)	0.6 (−)
		Negative Electrode	12.0 (−13%)	5.6 (−12%)	2.6 (−41%)	2.3 (−7%)	1.8 (−)	0.6 (−)
		Middlings	13.8 (−)	6.4 (−)	2.9 (−34%)	1.7 (−32%)	1.8 (−)	0.6 (−)
JSC-1A	Raw	n/a	18.8	6.8	3.2	3.3	3.4	0.5
	Al	Positive Electrode	18.8 (−)	6.8 (−)	2.8 (−11%)	3.5 (+7%)	3.2 (−7%)	0.5 (−)
		Negative Electrode	18.8 (−)	6.8 (−)	3.2 (−)	3.3 (−)	3.4 (−)	0.44 (−12%)
		Middlings	18.8 (−)	6.8 (−)	3.2 (−)	3.3 (−)	3.4 (−)	0.44 (−12%)
	Cu	Positive Electrode	19.9 (+6%)	6.8 (−)	2.8 (−11%)	3.3 (−)	3.4 (−)	0.44 (−12%)
		Negative Electrode	18.8 (−)	5.5 (−19%)	4.2 (+30%)	3.07 (−7%)	3.2 (−7%)	0.44 (−12%)
		Middlings	18.8 (−)	6.8 (−)	3.2 (−)	3.5 (+7%)	3.4 (−)	0.63 (+25%)
	PTFE	Positive Electrode	18.8 (−)	7.4 (+9%)	2.7 (−15%)	3.10 (−6%)	3.2 (−7%)	0.38 (−12%)
		Negative Electrode	18.8 (−)	6.8 (−)	3.8 (+18%)	3.3 (−)	3.4 (−)	0.5 (−)
		Middlings	18.8 (−)	6.8 (−)	3.0 (−6%)	3.3 (−)	3.4 (−)	0.63 (+25%)
KSC-1	Raw	n/a	12.3	5.2	3.1	1.1	–	2.8
	Al	Positive Electrode	13.7 (+11%)	4.0 (−23%)	4.1 (+31%)	1.1 (−)	–	3.9 (+40%)
		Negative Electrode	14.1 (+15%)	5.2 (−)	3.1 (−)	0.6 (−43%)	–	1.7 (−38%)
		Middlings	14.4 (+17%)	5.5 (+6%)	2.8 (−9%)	0.3 (−69%)	–	1.5 (−48%)
	Cu	Positive Electrode	13.7 (+11%)	5.2 (−)	2.3 (−27%)	1.1 (−)	–	1.90 (−32%)
		Negative Electrode	12.3 (−)	4.8 (−8%)	2.9 (−7%)	2.0 (+86%)	–	3.2 (+14%)
		Middlings	14.8 (+20%)	5.9 (+13%)	2.8 (−10%)	1.2 (+11%)	–	1.8 (−34%)
	PTFE	Positive Electrode	11.4 (−7%)	6.8 (+30%)	3.1 (−)	1.4 (+27%)	–	4.1 (+46%)
		Negative Electrode	12.3 (−)	5.2 (−)	3.5 (+13%)	0.75 (−32%)	–	2.1 (−26%)
		Middlings	15.1 (+23%)	6.1 (+18%)	3.1 (−)	0.70 (−36%)	–	1.93 (−31%)

per plate. This arrangement is then used to further analyse JSC-1A (although the published results are, surprisingly, identical to those reported in (Trigwell et al., 2009)), as well as NU-LHT-2M (with 5 *wt*.% added ilmenite), Apollo 14 14163 regolith and Apollo 17 70051 regolith.

For the NU-LHT-2M tests, the authors report XPS data supporting titanium and iron enrichment (+67% and +33%, respectively, for all particle sizes; +31% and +6% for the 75–100 *μm* fraction, respectively) (Trigwell et al., 2012). The Apollo 14 regolith was found to separate optimally with ±15 kV applied to the electrodes in combination with the aluminium tribocharger (Trigwell et al., 2012). The data from the XPS analysis of the material from each collection hopper indicates that titanium and iron enrichment of up to +164% and +12%, respectively, are possible (Trigwell et al., 2012). Considering that the Apollo 14 regolith contains only around 1.3% ilmenite by volume (French et al., 1991), these results suggest that tribocharging and parallel plate separation is a viable approach for lunar mineral beneficiation.
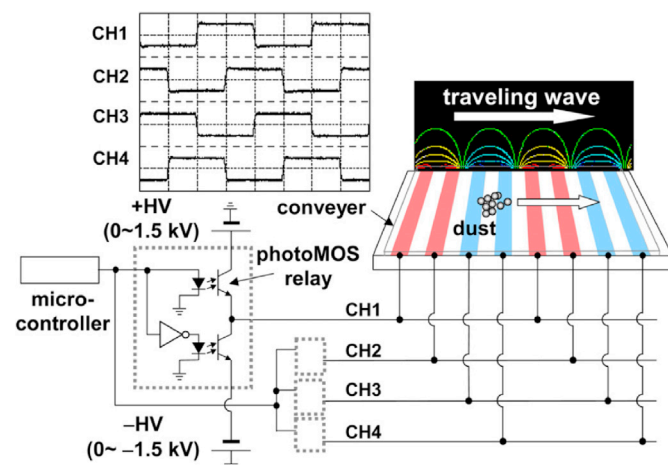

Fig. 7. Kawamoto et al.'s electrostatic travelling wave. Staggered, alternating voltages are sent by the microcontroller to the embedded electrodes (red and blue). The resulting non-uniform field interacts with the charged and neutral particles causing motion (Kawamoto et al., 2011).

Details regarding the mass of material collected in each hopper are not reported for these tests, making it impossible to evaluate the grade and recovery performance of the separator. Further, the experimental parameters (electrode potential, tribocharger material) are not reported, nor are the XPS measurements of the unbeneficiated material.

The Apollo 17 regolith was processed using multiple passes through the separator in an attempt to maximise the ilmenite collected; the bins with the highest ilmenite concentration were re-processed. The first pass was conducted with ±12 kV on the electrodes; the second and third passes were performed with ±24 kV (Trigwell et al., 2012). Trigwell et al. report the results of the first and third pass in *vol*.% per bin, but fail to report any details of the mass of material collected, preventing analysis of the grade and recovery. The authors state that "after the third run, the ilmenite concentration [had] significantly increased to 11.5% [*vol*.%] … [compared] with the feedstock, this represents a 311% increase [from 2.8 *vol*.%] after three passes" (Trigwell et al., 2012). This analysis, however, is invalid, as volumetric data alone is insufficient for evaluating the grade of the concentrate.

Quinn and colleagues (Quinn et al., 2012) adapted the apparatus as used by Trigwell et al., 2006, 2009, 2012 and Captain et al. (2007) for testing on low-gravity parabolic flights (see Fig. 6). The main differences in the set-up were that: aluminium was the only material used for tribocharging; testing was no longer performed under vacuum; and, the collector bin design was optimised following lab testing to maximise separation efficiency (Quinn et al., 2012). Experiments were performed over two flights, and aimed to test the effects of lunar gravity as well as the electrostatic field strength on the efficacy of the separator. The first flight applied ±8, ±10 and ± 12 kV to the electrodes, and the second used ±13, ±15 and ± 20 kV. The first battery of tests used as-received <1 *mm* NU-LHT-2M. The second battery used the same simulant as a base, however it had 10 *wt*.% ilmenite added to ensure that it could be detected in significant quantities during analysis, and was dried for 24 h prior to testing to drive off any adsorbed moisture (Quinn et al., 2012).

Analysis of the data from the first flight resulted in a statistically-significant difference between the amount of ilmenite found in the central and positive electrode bins compared to the negative bin; this was true across all three voltages (Quinn et al., 2012). Further, in agreement with Li et al. (1999), this indicates that ilmenite attains either no charge
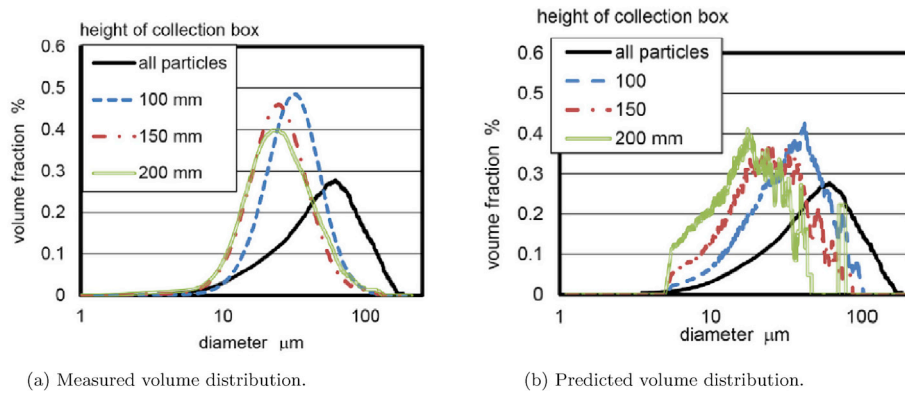
(a) Measured volume distribution.

(b) Predicted volume distribution.

Fig. 8. Measured (a) and predicted (b) volume distribution of particles in each of three collector boxes at different heights (Adachi et al., 2017a).

or a minimal positive charge. The enrichment of ilmenite was found to be as high as 60.3% with 69.4% recovery following a single pass under nominal testing conditions (Quinn et al., 2012). The second flight, using the amended simulant, found that ilmenite could be enriched by up to 106% following a single pass (approximately 10 *wt.*% to 20.6 *wt.*%), although only 23.9% of the original ilmenite was recovered (Quinn et al., 2012). It appears, however, that the authors have not accounted for the pre-existing ilmenite in NU-LHT-2M in their calculations. Employing the same method that they used earlier for determining grade, we find a more modest increase of 69.6%. The statistical significance of these data are not reported.

Across both flights, the data indicate that higher voltages result in higher-grade ilmenite. The recovery, however, was superior for the lower-voltage tests (69.4% at ±12 *kV* vs 23.9% at ±20 *kV*) (Quinn et al., 2012). Given the differences between the testing parameters of the two flights, it is not possible to conclude definitively that electrode voltage alone is responsible for either the upgrading or rate of recovery.

Considered together, the data from these studies indicate that tribocharging in conjunction with free-fall parallel plate separators are suited to mineral enrichment for lunar SRU. Further, it employs simple, light-weight and low-mass components, and has been tested in more environmental conditions than any other method. There are, however, gaps and inconsistencies in the data that detract from the successes that are reported.

4.1.3. Electrostatic Travelling Wave

Kawamoto, Adachi and their colleagues at Waseda University (Kawamoto and Seki, 2004; Adachi et al., 2016, 2017a, 2017b; Kawamoto, 2008, 2011, 2012; Kawamoto and Miwa, 2011; Kawamoto et al., 2011; Kawamoto and Shibata, 2015; Kawamoto and Guo, 2018; Kawamoto and Hashime, 2018; Adachi and Kawamoto, 2017) have demonstrated particle sizing and transport using to the so-called Electrostatic

Travelling Wave (ETW), shown in Fig. 7. The ETW uses alternating voltages sent by the microcontroller to embedded electrodes, thereby generating a non-uniform electrostatic field. Particles are charged tribostatically between themselves and through contact with the conveyor surface. The charged particles are then impelled through their interactions with the moving field.

Starting with uncharged carrier particles used in the electrophotography industry, Kawamoto et al. (Kawamoto and Seki, 2004) found that as they settled on the acetate rayon surface of the conveyor, a charge −0.01 and −0.03 *μC/g* was gained through tribocharging (Kawamoto and Seki, 2004). When the travelling wave was initialised, this charge was enough for the Coulomb force to become dominant and drive their motion. As they moved, they gained additional charge through tribocharging as they collided with other particles and the insulation, augmenting the Coulomb force (Kawamoto and Seki, 2004).

Kawamoto, Adachi and colleagues have successfully used this technology in a number of novel ways for space applications, such as the removal of lunar regolith simulants FJS-1 (a simulant of Japanese origin similar to JSC-1A), JSC-1A and terrestrial desert sand from solar panels (Kawamoto et al., 2011; Kawamoto and Shibata, 2015; Kawamoto and Guo, 2018; Kawamoto and Hashime, 2018) and a fluidless vacuum-like spacesuit cleaner (Kawamoto, 2008, 2011). For lunar mineral beneficiation, this technique has been successfully demonstrated for use in mineral size sorting by Adachi et al. (2017a).

Adachi et al. (2017a) investigated the use of the ETW for size-sorting FJS-1 particles from the <106 *μm* fraction in both air and vacuum. Numerical modelling and experimental results demonstrated the impracticality of this process in air, as fluid drag strongly influenced particle motion. Under vacuum, the authors were able to demonstrate experimentally that particles could be transported to collection hoppers positioned 100, 150 and 200 *mm* above the conveyor (Fig. 8a). These results agreed reasonably well with their theoretical model (Fig. 8b), and

(a) Predicted travel height by size.

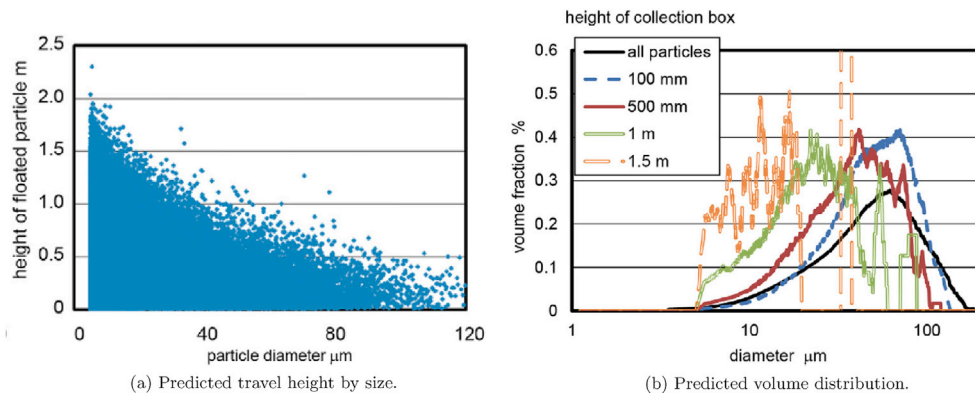(b) Predicted volume distribution.

Fig. 9. Modelling of particle travel height (a) and (b) volume distribution collected material (Adachi et al., 2017a).

suggest that this method would be ideal for the size sorting of small particles.

The authors go on to model the operation of this size sorter under lunar gravity. By assuming the same charge distribution, they predicted the maximum height that particles could theoretically be transported (Fig. 9a), and used this information to determine appropriate collection box heights (100, 500, 1000 and 1500 mm). By adapting the volume distribution model to lunar gravity, the authors found that particles could be collected in relatively discreet size fractions (Fig. 9b), and could even effectively separate very fine (around 10 μm) particles (Adachi et al., 2017a).

4.2. Magnetic separation

Magnetic separation is commonly used in terrestrial mineral processing, particularly for the removal of tramp iron from mineral streams, and for the separation of magnetite and roasted hematite and siderite from silica (Wills and Finch, 2015). As the lunar regolith contains both ferromagnetic and paramagnetic components, several beneficiation techniques have been presented in the literature for both early-stage sizing and gangue removal as well as for the enrichment of specific minerals.

In the lunar regolith, metallic nano-phase iron (np-Fe^0) is the dominant ferromagnetic phase (Runcorn et al., 1970). Early studies of Apollo samples found Fe^0 concentrations in the lunar soil to be an order of magnitude higher than within the rocks from which the soil formed (Taylor et al., 2005). It has been shown that this np-Fe^0 is vapour-deposited upon individual soil grains, forming iron-rich patinas (Keller and McKay, 1993, 1997; Pieters et al., 2000; Sasaki et al., 2001). In mature soils, this patina has been found on >90% of particles in the <10 μm fraction (Pieters et al., 2000; Keller et al., 1999). Further, np-Fe^0-bearing agglutinates comprise up to 80% of the <20 μm (dust) fraction, representing around 20% of the regolith (McKay et al., 1991; Liu et al., 2007).

Oder & Taylor (Oder and Taylor, 1990), using a Frantz isodynamic separator, found moderate success with magnetic separation of iron oxide and ilmenite from pyroxene (also paramagnetic). From immature lunar highland soil sample 67511, they recovered 22 wt.% of the sample

Table 8
Summary of previous work on lunar dry beneficiation.

Category	Process	Target Mineral	Fraction (μm)	Feed	Testing Conditions	Ref.
Gravitational	Size Sorting	n/a	75–150	JSC-1A NU-LHT-2M OB-1	Vacuum Lunar-g	Wilkinson (2011)
	Enrichment	n/a	n/a	n/a	n/a	None.
Magnetic	Size Sorting	n/a	n/a	n/a	n/a	None.
	Enrichment	Ilmenite	20–200	n/a	n/a	Williams et al. (1979)
		Anorthite	>150 45–150	Apollo 64421	No data	Oder et al. (1989)
		Ilmenite	90–150 45–90	Apollo 10058 Apollo 71055	No data	Taylor et al. (1992)
		Ilmenite Iron Oxide	150–425	Custom JSC-1A NU-LHT-2M	Vacuum	Berggren et al. (2011)
Electrostatic	Size Sorting	n/a	<106	FJS-1	Air, Vacuum	Adachi et al. (2017a)
	Size Sorting & Enrichment	Ilmenite	90–150	KSC-1 Apollo 10084	Air	Agosto (1984)
		Ilmenite	20–200	n/a	n/a	Williams et al. (1979)
	Enrichment	Ilmenite	<45 45–90 90–150 150–250 250–500	Custom	Air, N₂, Vacuum Heated: 100–200 °C Washed Samples	Agosto (1983)
		Ilmenite	90–150 150–200	KSC-1 Apollo 10084	Air, N₂, Vacuum Heated: 100–200 °C Washed Samples	Agosto (1985)
		n/a	50–75	JSC-1	Vacuum	Captain et al. (2007)
		Ilmenite	75–106	Custom	Air	Li et al. (1999)
		Ilmenite	<1000	NU-LHT-2M (+ilmenite)	Air Lunar-g	Quinn et al. (2012)
		n/a	<25 >100	JSC-1 MLS-1	Air	Trigwell et al. (2006)
		Ilmenite	50–75	JSC-1 JSC-1A KSC-1	Air, Vacuum	Trigwell et al. (2009)
		Ilmenite	50–75 75–100	JSC-1A NU-LHT-2M Apollo 14163 Apollo 70051	Vacuum	Trigwell et al. (2012)
		n/a	210–420 104–420	Custom	Vacuum Heated: 100–104 °C	Fraas (1970)

having a native FeO content of 0.6 *vol*.% (Oder and Taylor, 1990), and from an immature mare sample, 71061, they removed 57% of the ilmenite (Oder and Taylor, 1990) (initially 5.6 *vol*.% of the 90–150 μm fraction (Heiken and McKay, 1974)). Taylor et al. (1992) demonstrated that ilmenite from the 90–150 μm fraction of sample 10058 could be upgraded from 16% to a maximum of around 52%. In the 45–90 μm fraction of Apollo samples 10058 and 71055, they were able to achieve ilmenite concentrations of 62% and 72%, respectively. Further, Oder (1991) notes that as soil maturity increases, the proportion of magnetic constituents in the regolith increases as well, making it more challenging to separate out ilmenite from iron-rich pyroxene and agglutinates. The authors reported that the efficiency decreased with particles below 45 μm (Taylor et al., 2005).

Given the large fraction of ferromagnetic material in both the lunar dust and agglutinates, Taylor et al. (2005) suggest that hand-held permanent magnets could be a relatively simple way to remove the problematic dust fraction and agglutinates from the feed prior to subsequent enrichment stages. Reflecting on the work of Oder & Taylor (Oder and Taylor, 1990), the authors explain that the decrease in efficiency experienced in magnetically separating regolith fines was due to the higher magnetic susceptibility of the np-Fe^0-rich <50 μm fraction compared to that of coarser fractions (Taylor et al., 2005).

Separately, Kawamoto & Inoue (Kawamoto and Inoue, 2012) have demonstrated the use of permanent magnets for removing <53 μm FJS-1 particles embedded in spacesuit fabric. The authors successfully removed between 50 and 70% of the simulant from the fabric (Kawamoto and Inoue, 2012). They expect this to be higher with real regolith, however, as FJS-1 has both a lower relative magnetic permeability compared to the lunar regolith (1.073 for FJS-1 (Kawamoto and Inoue, 2012) versus 1.311 for regolith (Liu et al., 2007)) and higher a proportion of non-magnetic components.

Berggren et al. (2011) have explored the use of grade N-50 neodymium-iron-boron permanent magnets for enriching magnetic and paramagnetic materials from binary mixtures and lunar simulants. The authors report successfully enriching iron oxide from quartz sand (10 *wt*.% to 87 *wt*.%, two passes) and ilmenite from quartz sand (10 *wt*.% to 75 *wt*.%, three passes) (Berggren et al., 2011). The masses of the concentrate and tailings are not published, so it is not possible to evaluate recovery. Success with the simulants, however, was more modest. Effectively no upgrading was realised with JSC-1A. With NU-LHT-2M, iron oxide-rich minerals were upgraded from 4 *wt*.% in the feed to 10.5 *wt*.% in the concentrate stream (Berggren et al., 2011). Again, the mass of material collected was not published, making it impossible to properly evaluate the effectiveness.

Magnetic separation at scale for metal and oxygen production has been studied conceptually. Agosto (1981) calculated that magnetic separation could produce of up to 500 *t* of lunar iron-nickel alloy per annum, largely from the ferromagnetic fines. Oder (1991) has detailed a magnetic separation system for mare ilmenite concentration that could theoretically be used produce 1 *kt* of O2 by hydrogen reduction; this design, however, assumes a 100% efficient hydrogen reduction step, and would require the magnetic scalping system to treat up to 11.2 *t/ h*.

4.3. Summary

Table 8 summarises the experimental investigations described in this review on dry beneficiation of lunar regolith and simulants.

From this table, four key themes emerge:

1. Electrostatic methods have been studied the most;
2. Ilmenite has been the main mineral of interest for enrichment;
3. Size separation has been largely overlooked; and,
4. The fine (<50m) size fraction is not investigated often.

5. Conclusions

The future of long-duration deep-space exploration will be dependent on the ability to produce commodities, specifically oxygen, in space. Regardless of the reduction technique used, oxygen production on the Moon will require a beneficiated feedstock. In this review, the main dry beneficiation processes for lunar applications have been presented, and the results of those studies compared. The majority of research to date has focused on electrostatic separation.

The development of beneficiation and reduction technologies has been done independently. The feedstock requirements (namely mineralogy and size fraction) for the various reduction steps are often not specified, and as a result, most beneficiation research has focused on upgrading minerals without any specific targets beyond maximising grade. Beneficiation and reduction are, by nature and necessity, coupled, and must be developed as such.

To assist the lunar beneficiation research community, this review highlights several gaps that must be considered moving forward:

1. Whilst ilmenite is necessary for hydrogen reduction, optimisation by feed mineralogy has yet to be determined for alternative reduction methods such as molten salt electrolysis. Optimising beneficiation methods for one mineral may be short-sighted.
2. Standard methods for data reporting and evaluation have not been adopted by the SRU community. Terrestrial mineral processing employs standardised methods for evaluating processes based on mass balancing. Hadler et al. (2019) provide a set of standard language for reporting process parameters and experimental results. The adoption of this language will allow for meaningful comparisons to be drawn between works, and will facilitate the communication of up- and down-stream equipment requirements.
3. Size separation of regolith particles has been largely overlooked, however most reduction processes have yet to be optimised with respect to particle size.
4. Many of the electromagnetic properties for lunar minerals have not been determined empirically. Further, these values need be determined for samples of lunar origin, given the fundamental chemical differences between lunar and terrestrial minerals.
5. The fine (<50μm) size fraction often is not used for experimental trials, despite comprising over 40% of the regolith itself.

Appendix A. Supplementary data

Supplementary data to this article can be found online at https://doi.org/10.1016/j.pss.2020.104879.

References

Adachi, M., Kawamoto, H., 2017. Electrostatic sampler for large regolith particles on asteroids. J. Aero. Eng. 30 (3), 04016098.
Adachi, M., Maezono, H., Kawamoto, H., 2016. Sampling of regolith on asteroids using electrostatic force. J. Aero. Eng. 29 (4), 04015081.

Adachi, M., Moroka, H., Kawamoto, H., Wakabayashi, S., Hoshino, T., 2017a. Particle-size sorting system of lunar regolith using electrostatic traveling wave. J. Electrost. 89, 69–76.

Adachi, M., Hamazawa, K., Mimuro, Y., Kawamoto, H., 2017b. Vibration transport system for lunar and martian regolith using dielectric elastomer actuator. J. Electrost. 89, 88–98.

Afshar-Mohajer, N., Damit, B., Wu, C.-Y., Sorloaica-Hickman, N., 2011a. Efficiency evaluation of an electrostatic lunar dust collector. In: 41st International Conference on Environmental Systems, p. 5201.

Afshar-Mohajer, N., Damit, B., Wu, C.-Y., Sorloaica-Hickman, N., 2011b. Electrostatic particle collection in vacuum. Adv. Space Res. 48 (5), 933–942.

Agosto, W.N., 1981. Beneficiation and powder metallurgical processing of lunar soil metal. In: 4th Space Manufacturing; Proceedings of the Fifth Conference, p. 3263.

Agosto, W.N., 1983. Electrostatic separation of binary comminuted mineral mixtures. Space Manufacturing 315–334, 1983.

Agosto, W.N., 1984. Electrostatic separation and sizing of ilmenite in lunar soil simulants and samples. In: Lunar and Planetary Science Conference, vol. 15, pp. 1–2.

Agosto, W.N., 1985. Electrostatic concentration of lunar soil minerals. In: Lunar Bases and Space Activities of the 21st Century, p. 453.

Agosto, W.N., 1992. Lunar beneficiation. Space Resources - Materials 153–160.

Alshibli, K.A., Hasan, A., 2009. Strength properties of jsc-1a lunar regolith simulant. J. Geotech. Geoenviron. Eng. 135 (5), 673–679.

Arslan, H., Batiste, S., Sture, S., 2009. Engineering properties of lunar soil simulant jsc-1a. J. Aero. Eng. 23 (1), 70–83.

Bailey, A., 1984. Electrostatic phenomena during powder handling. Powder Technol. 37 (1), 71–85.

Ballantyne, G.R., 2011. Application of Dielectrophoresis to Mineral Processing. Thesis. University of Queensland.

Ballantyne, G.R., Holtham, P.N., 2010. Application of dielectrophoresis for the separation of minerals. Miner. Eng. 23 (4), 350–358. https://doi.org/10.1016/j.mineng.2009.09.001.

Ballantyne, G.R., Holtham, P.N., 2014. Evaluation of the potential for using dielectrophoresis to separate minerals. Miner. Eng. 55, 75–79.

Barthelemy, R., Mora, R.G., 1960. Electrical high tension minerals beneficiation: principles and technical aspects. Proceedings of the Vth International Mineral Processing Congress 36, 757–773.

Basu, A., Wentworth, S., McKay, D., 2001. Submillimeter grain-size distribution of apollo 11 soil 10084. Meteoritics Planet Sci. 36 (1), 177–181.

Baytekin, H., Patashinski, A., Branicki, M., Baytekin, B., Soh, S., Grzybowski, B.A., 2011. The mosaic of surface charge in contact electrification. Science 333 (6040), 308–312.

Berggren, M., Zubrin, R., Jonscher, P., Kilgore, J., 2011. Lunar soil particle separator. In: 49th AIAA Aerospace Sciences Meeting Including the New Horizons Forum and Aerospace Exposition, p. 436.

Bittner, J.D., Hrach, F., Gasiorowski, S., Canellopoulus, L., Guicherd, H., 2014. Triboelectric belt separator for beneficiation of fine minerals. Procedia Engineering 83, 122–129.

Brands, L., Beier, P., Stahl, I., 2001. Electrostatic Separation. Wiley Online Library, pp. 423–441.

Butler, R.F., 2004. Paleomagnetism: Magnetic Domains to Geologic Terranes, electronic edition Edition, vol. 319. Blackwell Scientific Publications Boston.

Captain, J., Trigwell, S., Arens, E., Biris, A., Captain, J., Quinn, J., Calle, C., 2007. Tribocharging lunar simulant in vacuum for electrostatic beneficiation. In: AIP Conference Proceedings, vol. 880. AIP, pp. 951–956.

Carr, B., 1963. Recovery of water or oxygen by reduction of lunar rock. AIAA J. 1 (4), 921–924.

Carrier III, W.D., 2003. Particle size distribution of lunar soil. J. Geotech. Geoenviron. Eng. 129 (10), 956–959.

Carrier III, W.D., 2005. The Four Things You Need to Know about the Geotechnical Properties of Lunar Soil.

Carrier III, W.D., Mitchell, J.K., Mahmood, A., 1973. The relative density of lunar soil. In: Lunar and Planetary Science Conference Proceedings, vol. 4, p. 2403.

Chikazumi, S., Graham, C.D., 2009. Physics of Ferromagnetism, second ed., vol. 94. Oxford University Press on Demand.

Cilliers, J.J., Rasera, J.N., Hadler, K., 2020. Estimating the Scale of Space Resource Utilisation (Sru) Operations to Satisfy Lunar Oxygen Demand, Planetary and Space Science Under Review.

Clarke, A.C., 1950. Electromagnetic launching as a major contribution to space flight. J. Br. Interplanet. Soc. (JBIS) 9 (6), 261–267.

Colaprete, A., Schultz, P., Heldmann, J., Wooden, D., Shirley, M., Ennico, K., Hermalyn, B., Marshall, W., Ricco, A., Elphic, R.C., Goldstein, D., Summy, D., Bart, G.D., Asphaug, E., Korycansky, D., Landis, D., Sollitt, L., 2010. Detection of water in the lcross ejecta plume. Science 330 (6003), 463–468.

Dahlin, D.C., Rule, A.R., 1993. Magnetic Susceptibility of Minerals in High Magnetic Fields. US Department of the Interior, Bureau of Mines.

Davenport, W.G., King, M.J., Schlesinger, M.E., Biswas, A.K., 2002. Extractive Metallurgy of Copper. Elsevier.

Fraas, F., 1962. Electrostatic separation of granular materials. United States Department of the Interior, Bureau of Mines Bulletin 603.

Fraas, F., 1970. Factors Related to Mineral Separation in a Vacuum. United States Department of the Interior, Bureau of Mines. Report 7404.

Freitas, R.A., Gilbreath, W. (Eds.), 1982. Advanced Automation for Space Missions: Proceedings of the 1980 NASA/ASEE Summer Study. National Aeronautics and Space Administration.

French, B.M., Heiken, G., Vaniman, D., Schmitt, J. (Eds.), 1991. Lunar Sourcebook: A User's Guide to the Moon. CUP Archive.

Fuller, M., 1974. Lunar magnetism. Rev. Geophys. 12 (1), 23–70.

Galliford, G., 2005. Particle Shape of Toners and the Advantage of Using Chemical Toner Manufacturing Methods, Report. Galliford Consulting & Marketing.

Gao, W., Li, Z., Sammes, N., 2011. An Introduction to Electronic Materials for Engineers. World Scientific Publishing Company.

Gibson, M.A., Knudsen, C.W., 1985. Lunar oxygen production from ilmenite. In: Lunar Bases and Space Activities of the 21st Century, p. 543.

Gibson, M.A., Knudsen, C.W., July 1996. Apparatus for manufacture of oxygen from lunar ilmenite. US Patent 5, 536,378.

Goertz, C., 1989. Dusty plasmas in the solar system. Rev. Geophys. 27 (2), 271–292.

Goldwater, D., Stickler, B., Martinetz, L., Northup, T.E., Hornberger, K., Millen, J., 2019. Levitated Electromechanics: All-Electrical Cooling of Charged Nano-And Micro-particles. Quantum Science and Technology.

Gooding, D.M., Kaufman, G.K., 2011. Tribocharging and the triboelectric series. Encyclopedia of Inorganic and Bioinorganic Chemistry 1–9.

Gupta, R., Gidaspow, D., Wasan, D., 1993. Electrostatic separation of powder mixtures based on the work functions of its constituents. Powder Technol. 75 (1), 79–87.

Hadler, K., Martin, D., Carpenter, J., Cilliers, J., Morse, A., Starr, S., Rasera, J., Seweryn, K., Reiss, P., Meurisse, A., 2019. A universal framework for space resource utilisation (sru). Planet. Space Sci. 104811.

Heiken, G., 1975. Petrology of lunar soils. Rev. Geophys. 13 (4), 567–587.

Heiken, G., McKay, D., 1974. Petrology of apollo 17 soils. 5th lunar planet sci. In: Proceedings of the 5th Lunar and Planetary Science Conference, Houston, pp. 843–860.

Hill, E., Patchen, A., Deane, B., Liu, Y., Park, J., Taylor, L., 2006. Lunar simulants as feedstocks for isru processing: mineralogy and chemistry. In: Earth & Space 2006: Engineering, Construction, and Operations in Challenging Environment, pp. 1–8.

Hill, E., Mellin, M.J., Deane, B., Liu, Y., Taylor, L.A., 2007. Apollo sample 70051 and high-and low-ti lunar soil simulants mls-1a and jsc-1a: implications for future lunar exploration. J. Geophys. Res.: Plan 112 (E2).

Horányi, M., 1996. Charged dust dynamics in the solar system. Annu. Rev. Astron. Astrophys. 34 (1), 383–418.

Inculet, I., 1979. Electrostatic separation of lunar soil. In: 4th Conference on Space Manufacturing Facilities. Princeton University, p. 1378.

Inculet, I.I., Bergougnou, M.A., Bauer, S., 1972. Electrostatic beneficiation apparatus for fluidized iron and other ores. IEEE Trans. Ind. Appl. (6), 744–748.

Ireland, P.M., 2010a. Triboelectrification of particulate flows on surfaces: Part i—experiments. Powder Technol. 198 (2), 189–198.

Ireland, P.M., 2010b. Triboelectrification of particulate flows on surfaces: Part ii—mechanisms and models. Powder Technol. 198 (2), 199–210.

Ireland, P.M., 2012. Dynamic particle-surface tribocharging: the role of shape and contact mode. J. Electrost. 70 (6), 524–531.

Ireland, P.M., Nicholson, K., 2011. Analysis and comparison of particle tribochargers. Miner. Eng. 24 (8), 914–922.

Izvekova, Y.N., Popel, S., 2013. Adhesion of rough particles of lunar regolith. EPSC Abstr 8, 1–2.

Jackson, R., 2015. John tyndall and the early history of diamagnetism. Ann. Sci. 72 (4), 435–489.

Jones, T.B., 1979. Dielectrophoretic force calculation. J. Electrost. 6 (1), 69–82.

Just, G., Smith, K., Joy, K., Roy, M., 2020. Parametric review of existing regolith excavation techniques for lunar in situ resource utilisation (isru) and recommendations for future excavation experiments. Planet. Space Sci. 180, 104746.

Kawamoto, H., 2008. Some techniques on electrostatic separation of particle size utilizing electrostatic traveling-wave field. J. Electrost. 66 (3–4), 220–228.

Kawamoto, H., 2011. Electrostatic cleaning device for removing lunar dust adhered to spacesuits. J. Aero. Eng. 25 (3), 470–473.

Kawamoto, H., 2012. Sampling of small regolith particles from asteroids utilizing an alternative electrostatic field and electrostatic traveling wave. J. Aero. Eng. 27 (3), 631–635.

Kawamoto, H., Guo, B., 2018. Improvement of an electrostatic cleaning system for removal of dust from solar panels. J. Electrost. 91, 28–33.

Kawamoto, H., Hashime, S., 2018. Practical performance of an electrostatic cleaning system for removal of lunar dust from optical elements utilizing electrostatic traveling wave. J. Electrost. 94, 38–43.

Kawamoto, H., Inoue, H., 2012. Magnetic cleaning device for lunar dust adhering to spacesuits. J. Aero. Eng. 25 (1), 139–142.

Kawamoto, H., Miwa, T., 2011. Mitigation of lunar dust adhered to mechanical parts of equipment used for lunar exploration. J. Electrost. 69 (4), 365–369.

Kawamoto, H., Seki, K., 2004. Mechanism on traveling-wave transport of particles. In: NIP & Digital Fabrication Conference. Society for Imaging Science and Technology, pp. 1019–1026.

Kawamoto, H., Shibata, T., 2015. Electrostatic cleaning system for removal of sand from solar panels. J. Electrost. 73, 65–70.

Kawamoto, H., Uchiyama, M., Cooper, B., McKay, D., 2011. Mitigation of lunar dust on solar panels and optical elements utilizing electrostatic traveling-wave. J. Electrost. 69 (4), 370–379.

Keller, L.P., McKay, D.S., 1993. Discovery of vapor deposits in the lunar regolith. Science 261 (5126), 1305–1307.

Keller, L.P., McKay, D.S., 1997. The nature and origin of rims on lunar soil grains. Geochem. Cosmochim. Acta 61 (11), 2331–2341.

Keller, L., Wentworth, S., McKay, D., Taylor, L., Pieters, C., Morris, R., 1999. Space weathering in the fine size fractions of lunar soils: soil maturity effects. In: New Views of the Moon 2: Understanding the Moon through the Integration of Diverse Datasets, p. 32.

Kelly, E., Spottiswood, D., 1989a. The theory of electrostatic separations: a review - Part I: Fundamentals. Miner. Eng. 2 (1), 33–46.

Kelly, E., Spottiswood, D., 1989b. The theory of electrostatic separations: a review - Part II: Particle charging. Miner. Eng. 2 (2), 193–205.

Kelly, E., Spottiswood, D., 1989c. The theory of electrostatic separations: a review - Part III: The separation of particles. Miner. Eng. 2 (3), 337–349.

Kim, K., Elsayed-Ali, H.E., 1982. Investigation of Electron-Beam Charging for Inertial-Confinement-Fusion Targets. Charged Particle Research Laboratory Report No. 3-82, Tech. Rep. Lawrence Livermore National Lab., CA (USA); Illinois Univ., Urbana (USA.

Knoll, F., Taylor, J., 1985. Advances in electrostatic separation, Mining, Metallurgy & Exploration 2 (2), 106–114.

Labotka, T., Kempa, M.J., White, C., Papike, J., Laul, J., 1980. The lunar regolith-comparative petrology of the apollo sites. In: Lunar and Planetary Science Conference Proceedings, vol. 11, pp. 1285–1305.

Lacks, D.J., 2012. The unpredictability of electrostatic charging. Angew. Chem. Int. Ed. 51 (28), 6822–6823.

Lawver, J., Taylor, J., Knoll, F., 1986. Laboratory Testing for Electrostatic Concentration Circuit Design. Society of Mining Engineers, pp. 454–477 book section 30.

Li, T., Ban, H., Hower, J., Stencel, J., Saito, K., 1999. Dry triboelectrostatic separation of mineral particles: a potential application in space exploration. J. Electrost. 47 (3), 133–142.

Lin, T., Love, H., Stark, D., 1992. Physical properties of concrete made with apollo 16 lunar soil sample. Tech. Rep. N93–13987. NASA.

Lindley, K., Rowson, N., 1997a. Feed preparation factors affecting the efficiency of electrostatic separation. Phys. Separ. Sci. Eng. 8 (3), 161–173.

Lindley, K., Rowson, N., 1997b. Charging mechanisms for particles prior to electrostatic separation. Phys. Separ. Sci. Eng. 8 (2), 101–113.

Liu, C., Bard, A.J., 2008. Electrostatic electrochemistry at insulators. Nat. Mater. 7 (6), 505.

Liu, C.-y., Bard, A.J., 2009a. Electrons on dielectrics and contact electrification. Chem. Phys. Lett. 480 (4–6), 145–156.

Liu, C.-y., Bard, A.J., 2009b. Chemical redox reactions induced by cryptoelectrons on a pmma surface. J. Am. Chem. Soc. 131 (18), 6397–6401.

Liu, C.-y., Bard, A.J., 2010. Electrostatic electrochemistry: nylon and polyethylene systems. Chem. Phys. Lett. 485 (1–3), 231–234.

Liu, Y., Taylor, L.A., Thompson, J.R., Schnare, D.W., Park, J.-S., 2007. Unique properties of lunar impact glass: nanophase metallic fe synthesis. Am. Mineral. 92 (8–9), 1420–1427.

Lu, H., Li, J., Guo, J., Xu, Z., 2008. Movement behavior in electrostatic separation: recycling of metal materials from waste printed circuit board. J. Mater. Process. Technol. 197 (1–3), 101–108.

Manouchehri, H.-R., Hanumantha Rao, K., Forssberg, K., 2000a. Review of electrical separation methods - part 1: fundamental aspects. Mining, Metallurgy and Exploration 17 (1), 23–36.

Manouchehri, H.-R., Hanumantha Rao, K., Forssberg, K., 2000b. Review of electrical separation methods - part 2: practical considerations. Mining, Metallurgy & Exploration 17 (3), 139–166.

McKay, D.S., Heiken, G.H., Taylor, R.M., Clanton, U.S., Morrison, D.A., Ladle, G.H., 1972. Apollo 14 soils: size distribution and particle types. In: Lunar and Planetary Science Conference Proceedings, vol. 3, p. 983.

McKay, D.S., Heiken, G., Basu, A., Blanford, G., Simon, S., Reedy, R., French, B.M., Papike, J., 1991. The lunar regolith. In: Heiken, G.H., Vaniman, D.T., French, B.M. (Eds.), Lunar Sourcebook: A User's Guide to the Moon. Cambridge University Press, pp. 285–356. Ch. 7.

Meyer, C., 2003. The Lunar Petrographic Educational Thin Section Set.

Miller, M., Barringer, S., 2002. Effect of sodium chloride particle size and shape on nonelectrostatic and electrostatic coating of popcorn. J. Food Sci. 67 (1), 198–201.

Mora, R.G., 1958. Study of Electrical Concentration of Minerals, Thesis. Massachusetts Institute of Technology.

Mudd, G.M., Weng, Z., 2012. Base Metals. RSC Publishing, pp. 11–59.

Oder, R., 1991. Magnetic separation of lunar soils. IEEE Trans. Magn. 27 (6), 5367–5370.

Oder, R.R., Taylor, L.A., 1990. Magnetic beneficiation of highland and hi-ti mare soils - magnet requirements. In: Engineering, Construction, and Operations in Space II, vol. 1, pp. 133–142.

Oder, R., Taylor, L., Keller, R., 1989. Magnetic characterization of lunar soils. In: Lunar and Planetary Science Conference, vol. 20, pp. 804–805.

Papike, J., Simon, S.B., Laul, J., 1982. The lunar regolith: chemistry, mineralogy, and petrology. Rev. Geophys. 20 (4), 761–826.

Parodi, F., 1996. Physics and Chemistry of Microwave Processing. Elsevier, pp. 669–728 book section Supplement 2 - (Chapter 19).

Pauthenier, M., Moreau-Hanot, M., 1932. La charge des particules sphériques dans un champ ionisé. J. Phys. Radium 3 (12), 590–613.

Perkins, S.W., Madson, C.R., 1996. Mechanical and load-settlement characteristics of two lunar soil simulants. J. Aero. Eng. 9 (1), 1–9.

Perko, H.A., Nelson, J.D., Sadeh, W.Z., 2001. Surface cleanliness effect on lunar soil shear strength. J. Geotech. Geoenviron. Eng. 127 (4), 371–383.

Pieters, C.M., Taylor, L.A., Noble, S.K., Keller, L.P., Hapke, B., Morris, R.V., Allen, C.C., McKAY, D.S., Wentworth, S., 2000. Space weathering on airless bodies: resolving a mystery with lunar samples. Meteoritics Planet Sci. 35 (5), 1101–1107.

Pohl, H.A., 1951. The motion and precipitation of suspensoids in divergent electric fields. J. Appl. Phys. 22 (7), 869–871.

Pohl, H.A., 1958. Some effects of nonuniform fields on dielectrics. J. Appl. Phys. 29 (8), 1182–1188.

Pohl, H.A., 1960. Nonuniform field effects in poorly conducting media. J. Electrochem. Soc. 107 (5), 386–390.

Pohl, H.A., 1978. Dielectrophoresis - the Behavior of Neutral Matter in Nonuniform Electric Fields. Cambridge University Press.

Quinn, J.W., Captain, J.G., Weis, K., Santiago-Maldonado, E., Trigwell, S., 2012. Evaluation of tribocharged electrostatic beneficiation of lunar simulant in lunar gravity. J. Aero. Eng. 26 (1), 37–42.

Ray, C., Reis, S., Sen, S., O'Dell, J., 2010. Jsc-1a lunar soil simulant: characterization, glass formation, and selected glass properties. J. Non-Cryst. Solids 356 (44–49), 2369–2374.

Rosenblum, S., Brownfield, I.K., 2000. Magnetic Susceptibilities of Minerals, Report Report 99-529. United States Geological Survey.

Runcorn, S., Collinson, D., O'Reilly, W., Battey, M., Stephenson, A., Jones, J., Manson, A., Readman, P., 1970. Magnetic properties of apollo 11 lunar samples. Geochem. Cosmochim. Acta Suppl. 1, 2369.

Sasaki, S., Nakamura, K., Hamabe, Y., Kurahashi, E., Hiroi, T., 2001. Production of iron nanoparticles by laser irradiation in a simulation of lunar-like space weathering. Nature 410 (6828), 555.

Scheeres, D.J., Hartzell, C.M., Sánchez, P., Swift, M., 2010. Scaling forces to asteroid surfaces: the role of cohesion. Icarus 210 (2), 968–984.

Schein, L., 2000. Electric field theory of toner charging. J. Imag. Sci. Technol. 44 (6), 475–483.

Schein, L., 2007. Recent progress and continuing puzzles in electrostatics. Science 316 (5831), 1572–1573.

Schrader, C., Rickman, D., McLemore, C., Fikes, J., Stoeser, D., Wentworth, S., McKay, D., 2009. Lunar regolith characterization for simulant design and evaluation using figure of merit algorithms. In: 47th AIAA Aerospace Sciences Meeting Including the New Horizons Forum and Aerospace Exposition, p. 755.

Schwandt, C., Hamilton, J.A., Fray, D.J., Crawford, I.A., 2012. The production of oxygen and metal from lunar regolith. Planet. Space Sci. 74 (1), 49–56.

Sibille, L., Carpenter, P., Schlagheck, R., French, R.A., 2006. Lunar regolith simulant materials: recommendations for standardization, production, and usage. Tech. rep., NASA Marshall Space Flight Center. Report Number: NASA/TP-2006-214605, M-1174. https://ntrs.nasa.gov/search.jsp?R=20060051776.

Sowers, G.F., 2016. A cislunar transportation system fueled by lunar resources. Space Pol. 37, 103–109.

Strangway, P.G., Olhoeft, D.W.G., 1977. Magnetic and dielectric properties of lunar samples. In: The Soviet-American Conference on the Cosmochemistry of the Moon and Planets, vol. 1, pp. 417–431. Part.

Stubbs, T.J., Vondrak, R.R., Farrell, W.M., 2006. A dynamic fountain model for lunar dust. Adv. Space Res. 37 (1), 59–66.

Svoboda, J., 1994. The effect of magnetic field strenght on the efficiency of magnetic separation. Miner. Eng. 7 (5–6), 747–757.

Taylor, L.A., Carrier III, W.D., 1993. Oxygen production on the moon: an overview and evaluation. Resources of Near-Earth Space 69.

Taylor, L., McKay, D., Graf, J., Patchen, A., Wentworth, S., Oder, R., Jerde, E., 1992. Magnetic beneficiation of high-ti mare basalts: petrographic analyses. In: Lunar and Planetary Science Conference, vol. 23.

Taylor, L.A., Patchen, A., Taylor, D.-H.S., Chambers, J.G., McKay, D.S., 1996. X-ray digital imaging petrography of lunar mare soils: modal analyses of minerals and glasses. Icarus 124 (2), 500–512.

Taylor, L., Schmitt, H., Carrier, W., Nakagawa, M., 2005. Lunar dust problem: from liability to asset. In: 1st Space Exploration Conference: Continuing the Voyage of Discovery, p. 2510.

Taylor, L.A., Pieters, C.M., Britt, D., 2016. Evaluations of lunar regolith simulants. Planet. Space Sci. 126, 1–7.

Trigwell, S., Captain, J., Captain, J., Arens, E., Quinn, J., Calle, C., 2006. Electrostatic Beneficiation of Lunar Simulant. NASA. Report.

Trigwell, S., Captain, J.G., Arens, E.E., Quinn, J.W., Calle, C.I., 2009. The use of tribocharging in the electrostatic beneficiation of lunar simulant. IEEE Trans. Ind. Appl. 45 (3), 1060–1067.

Trigwell, S., Captain, J., Weis, K., Quinn, J., 2012. Electrostatic beneficiation of lunar regolith: applications in situ resource utilization. J. Aero. Eng. 26 (1), 30–36.

U. S. G. Survey, 2008. Material Safety Data Sheet - NU-LHT-2m.

Wang, X., Schwan, J., Hsu, H.-W., Grün, E., Horányi, M., 2016. Dust charging and transport on airless planetary bodies. Geophys. Res. Lett. 43 (12), 6103–6110.

Washizu, M., 1993. Precise calculation of dielectrophoretic force in arbitrary field. J. Electrost. 29 (2), 177–188.

Washizu, M., Jones, T., 1994. Multipolar dielectrophoretic force calculation. J. Electrost. 33 (2), 187–198.

Wilkinson, A., 2011. Size Beneficiation of Regolith for Simplicity and Efficiency.

Williams, R.J., McKay, D.S., Giles, D., Bunch, T.E., 1979. Mining and beneficiation of lunar ores. Space Resources and Space Settlements 275–288.

Wills, B.A., Finch, J., 2015. Wills' Mineral Processing Technology: an Introduction to the Practical Aspects of Ore Treatment and Mineral Recovery. Butterworth-Heinemann.

Zafar, U., Alfano, F., Ghadiri, M., 2018. Evaluation of a new dispersion technique for assessing triboelectric charging of powders. Int. J. Pharm. 543 (1–2), 151–159.

Zeng, X., He, C., Wilkinson, A., 2010. Geotechnical properties of NU-LHT-2M lunar highland simulant. J. Aero. Eng. 23 (4), 213–218.